DIPLOMARBEIT

Wave Control in Complex Media: from System Design to Wave Front Shaping

ausgeführt am

Institut für Theoretische Physik
der Technischen Universität Wien

Institute for Theoretical Physics
Vienna University of Technology

unter der Anleitung von
Dipl.-Ing. Philipp Ambichl
und
Univ.-Prof. Dipl.-Ing. Dr. techn. Stefan Rotter
durch

Andre Brandstötter

andre.brandstoetter@student.tuwien.ac.at

Datum

Unterschrift

Contents

Chapter 1

Introduction

Wave propagation, wave scattering and all manifestations of fundamental wave behavior, such as interference or diffraction, have been fascinating physicists for a long time already [1, 2]. Whereas in the early years of wave physics much effort has been devoted to understanding the fundamental nature of waves, the goal nowadays is to manipulate and control waves so that they fulfill a certain function, such as imaging, detection and efficient transmission across disordered materials [3]. Most of the progress in the optical domain that has recently been made is due to the availability of spatial light modulators and spectral phase filters which can be used, e.g., to achieve a temporal and/or spatial focus behind a medium by shaping the incident wave front [4–9]. In addition to this notion, the idea of controlling the medium itself has been explored [10–17]. This second approach has a long history if we think, for example, of optical instruments such as lenses..

This thesis covers novel aspects of these two contrasting approaches that both aim to control waves in certain geometries, leading to previously unknown and counterintuitive wave phenomena. Whereas in the first part of this thesis wave scattering is controlled by delicately designing the refractive index of a scattering medium, in the second part we consider the scattering system as fixed and show how we can control the wave inside a geometry by shaping the wave front of the incident wave. The derivations in this thesis have been conducted for electromagnetic waves, however, all observations are also valid for matter waves, since the underlying wave equations, the stationary Schrödinger equation and the Helmholtz equation, are equivalent for unbounded scattering states. Therefore, the words "refractive index" and "potential" can be used as synonyms since they are just connected by an algebraic equation.

Our intuition tells us that waves traveling through a heterogenous material undergo multiple scattering processes leading to a highly fluctuating intensity profile. Controlling the wave effects that lead to this complex spatial profile of the wave is in high demand in many different disciplines of science and technology. In this context, the first part of this thesis covers fringe-free scattering states that can be obtained by adding a well-tailored gain/loss distribution to a non-uniform complex medium. In a recent work [18], a new class of non-uniform potentials with

well-balanced gain/loss regions was introduced that enables waves to have a fringe-free intensity pattern. These so-called constant-intensity (CI) waves were studied in the paraxial approximation in waveguide systems, in which the potential varies in transverse direction, but stays constant in longitudinal direction. In our work [19], the concept of constant-intensity waves was extended to scattering systems, in which the potential (or refractive index) varies in propagation direction, such that the paraxial approximation cannot be applied anymore. Starting from this point, this thesis provides a detailed characterization of these counterintuitive waves in order to gain a deeper understanding of this phenomenon. The connection to $\mathcal{PT}$-symmetry [20, 21] and unidirectional invisibility [22] is discussed, as well as possible experimental realizations.

Having shown that a proper design of the refractive index can lead to new wave effects, the second part of this thesis follows the opposing approach. The theoretical description of an experimental realization of so-called particle-like scattering states [23] in microwave cavities is one example of where wave front shaping can be useful. These beam-like scattering states have a number of fascinating properties like a broadband frequency stability, a highly collimated wave function also inside the considered scattering system and a deterministic value of transmission. Low-power and/or secure communication are just two of many possible applications of particle-like states. A quantitative description of all the imperfections that an experiment normally comes along with, such as absorption or noise, is included in our theoretical analysis. These particle-like states can be found among scattering states that have a well-defined delay time. Inspired by the method used to find time-delay eigenstates [23], we subsequently show that particle-like states are just one example of a more general concept that can be used in wave front shaping experiments to find states with specific properties. In a next step, we use this concept in order to focus an incoming wave onto an obstacle inside the scattering geometry, or just the opposite, to create a scattering state that occupies the entire scattering region except for the area around a chosen obstacle. Moreover, an algorithm leading to a possible experimental realization of a Coherent Perfect Absorber (CPA) [24–26], which is the time-reversed counterpart of a laser, is discussed in the last part of this thesis.

All three of the aforementioned wave front shaping projects, i.e., particle-like states, avoiding and focusing states as well as the CPA were conducted in collaboration with Ulrich Kuhl's group at the University of Nice, who has a strong expertise in microwave experiments. Whereas the first two projects have already led to promising preliminary measurement results, the CPA experiment is still in progress.

Chapter 2

Constant-Intensity Waves

2.1 Refractive Index Distribution

A wave traveling through a non-uniform medium generally results in a highly complex variation of it's spatial profile due to scattering, diffraction and interference. Controlling or suppressing these effects is one of the main tasks of wave physics, such as for cloaking devices [27], the research in adaptive optics [28] and in wave front shaping through complex media [3]. New and unconventional wave phenomena have been explored in non-Hermitian systems, i.e., systems with gain and loss, which serve as sources and sinks for waves [29, 30]. Inspired by this recent progress in non-Hermitian physics, a new class of non-uniform potentials with well-balanced gain/loss regions was introduced that enables waves to have a fringe-free intensity pattern [18]. These constant-intensity waves (CI waves) were introduced as solutions of the paraxial wave equation, where the potential varies only in transverse direction. The paraxial approximation ignores any backscattering from the potential and the phase of the incident wave has to be modulated through wave front shaping in order to get the desired constant-intensity wave. Contrary to this approach, we now examine constant-intensity waves in the full scattering problem that is governed by the Helmholtz equation and thus does not rely on any approximation (apart from smoothness of the potential). Furthermore, no wave front shaping of the incoming wave is necessary.

Our starting point is a scattering geometry composed of a one-dimensional (1D) slab located between $-L$ and L with a varying dielectric function $\epsilon(x)$,

$$\epsilon(x) = n^2(x) = [n_r(x) + jn_i(x)]^2, \tag{2.1}$$

where j represents the imaginary unit, $n_r(x)$ denotes the real part and $n_i(x)$ the imaginary part of the complex refractive index $n(x)$. A negative value for $n_i(x)$ corresponds to gain (amplification) and a positive value for $n_i(x)$ to loss (absorption) of the wave. When a wave is incident on a spatially varying refractive index $n(x)$, forward and backward propagating waves lead to a complex interference pattern. We now introduce a new class of complex refractive indices $n(x)$ that lead to a fringe-free intensity pattern for incident plane waves with a specific wavelength,

provided that $n_r(x)$ and $n_i(x)$ fulfill a certain relation. Our calculations are based on the Helmholtz equation in 1D,

$$[\triangle + n^2(x)k_0^2]\psi(x) = 0, \tag{2.2}$$

where $\triangle = \frac{d^2}{dx^2}$ is the Laplacian in 1D, k_0 the wavenumber in vacuum and $\psi(x)$ the linearly polarized component of the electric field. We now demand that the wave has a constant intensity inside the modulated potential region, therefore our ansatz is a wave with constant amplitude and a position-dependent phase

$$\psi(x) = e^{jk_0 \int_{x_0}^{x} W(x')\,\mathrm{d}x'}, \tag{2.3}$$

where $W(x)$ is a real auxiliary function and $x_0 = -L$ denotes the beginning of the potential region. Inserting ansatz (2.3) into the Helmholtz equation (2.2), provides us with the corresponding refractive index distribution

$$n^2(x) = W^2(x) - \frac{j}{k_0}\frac{dW(x)}{dx}. \tag{2.4}$$

Using perfect transmission boundary conditions at $x = \pm L$,

$$\left.\frac{d\psi}{dx}\right|_{L} = jk\psi(L), \left.\frac{d\psi}{dx}\right|_{-L} = jk\psi(-L) \tag{2.5}$$

leads to the following boundary conditions for the auxiliary function $W(x)$:

$$W(-L) = W(L) = 1. \tag{2.6}$$

The solution in entire space, i.e., including free space in front of and behind the potential region reads as follows,

$$\psi(x) = \begin{cases} \exp[jk_0\,(x+L)], & x < -L\,, \\ \exp[jk_0 \int_{-L}^{x} W(x')dx'], & -L \le x \le L\,, \\ \exp[jk_0\,(x-L)], & x > L, \end{cases} \tag{2.7}$$

where one can easily see that the wave has constant intensity, $I(x) = |\psi(x)|^2 = 1$, in the asymptotic regions (where $\epsilon(x) = 1$) as well as inside the scattering region where the dielectric constant varies. Hence, we show that one can identify the appropriate refractive index distribution $n(x)$ according to Eq. (2.4) such as the wave inside and outside of the potential region has constant intensity for incident plane waves with wavenumber k_0.

Furthermore, using Eq. (2.1) and Eq. (2.4), we derive analytical relations between $W(x)$ and the real and imaginary part of the refractive index $n(x)$:

$$\begin{aligned} n_r(x) &= \frac{W(x)}{\sqrt{2}}\left\{1 + \left[1 + \frac{W'^2(x)}{W^4(x)k_0^2}\right]^{\frac{1}{2}}\right\}^{\frac{1}{2}}, \\ n_i(x) &= -\frac{1}{2k_0}\frac{W'(x)}{n_r(x)}, \end{aligned} \tag{2.8}$$

with $W'(x) = \frac{dW(x)}{dx}$. From these equations we can see that we get $n_i(x) = 0$ only for the case that $W(x) = \text{const}$, which is the trivial case of a plane wave traveling in a uniform material. Thus, non-trivial constant-intensity waves of the form (2.3) can only exist in non-Hermitian systems featuring gain and loss. Also note that $W(x)$ has to be larger than 1 to ensure that $n_r(x) \geq 1$ as can be seen from Eq. (2.8).

We want to emphasize that we are able to obtain a CI refractive index not only by starting with a given generating function $W(x)$ from which $n_r(x)$ and $n_i(x)$ can be derived, but also from a given real part of the refractive index $n_r(x)$ from which the corresponding gain/loss part $n_i(x)$ can be found by an easy iterative scheme (not shown).

In order to elucidate the above ideas, we consider in the following a disordered system, which leads to Anderson localization of the incident wave. For a real and disordered systems larger than the localization length, it is very unlikely to get close to unit transmittance which occurs only at well-isolated resonant wavenumbers. Using the concept of CI waves we can turn this behavior upside down - in the sense that we can get perfect transmission at any predetermined wavenumber k_0. In this simulation, a disordered CI refractive index distribution is considered with a tunable imaginary component $\epsilon(x) = [n_r(x) + j\alpha n_i(x)]^2$. For $\alpha = 0$ the system is Hermitian and incident waves get localized with a localization length $\xi = -2L \left\langle ln[T(L)] \right\rangle^{-1}$, where $T = |t|^2$ is the transmittance of the wave and the brackets indicate an averaging process over many refractive index configurations. Fig. 2.1(b) shows the localization length ξ, whereas (a) and (c) show the real and imaginary part of the refractive index, respectively. In Fig. 2.1(e) we can see the intensity of scattering states for different values of the gain/loss strength α. Starting from the Hermitian case ($\alpha = 0$), where the wave is localized, we end up with a CI wave featuring perfect transmission when the full gain/loss strength ($\alpha = 1$) is reached. If, however, we add the gain-only distribution (negative part in Fig. 2.1(c)) to the Hermitian system, we also end up with a localized wave, as shown in Fig. 2.1(d), which indicates that the interplay of gain and loss is crucial for the emergence of constant-intensity waves.

Having derived the basic equations describing CI waves and having shown that CI waves can even exist in disordered systems, we can now gain a better understanding of this phenomenon. In the next section we would like to find out what happens to incident plane waves with detuned wavenumbers $k \neq k_0$. Is the emergence of constant intensity a phenomenon that appears abruptly at k_0 or is there a smooth transition? In other words, is there a sharp or a rather broad peak in the transmission spectrum $|t(k)|$ at k_0?

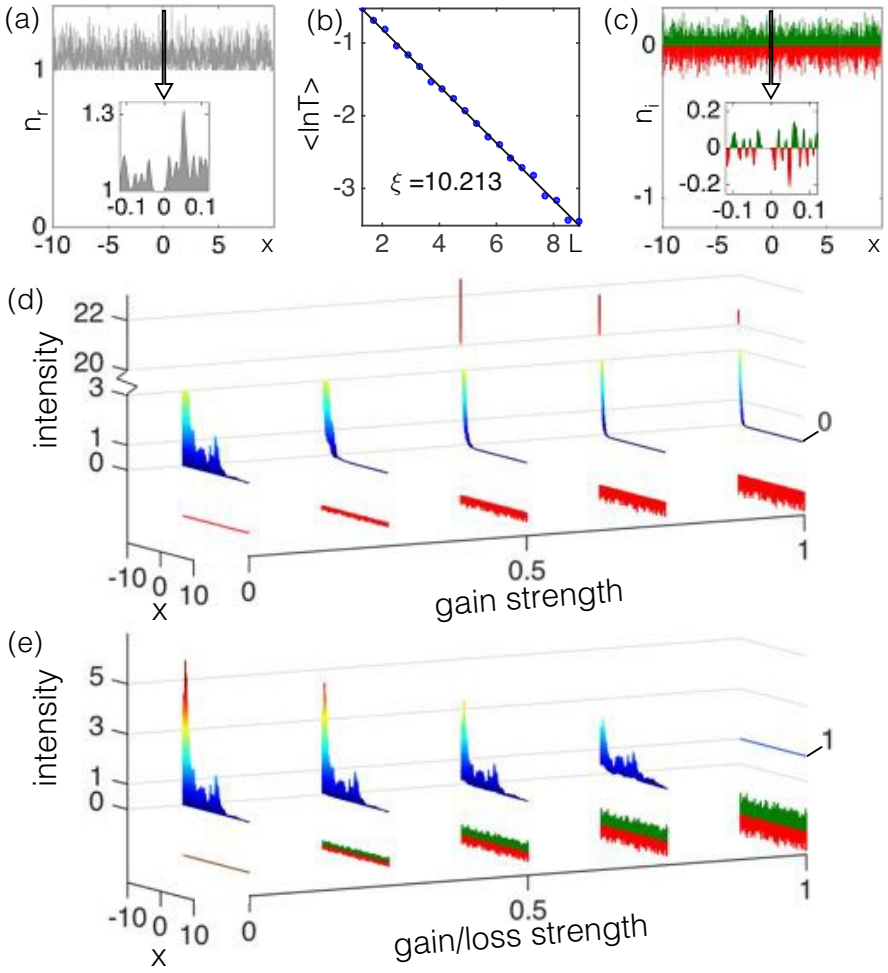

Figure 2.1: (a) Disordered Hermitian refractive index distribution $n_r(x)$ (gray) that leads to an exponential suppression of the transmittance T with a localization length ξ calculated in (b). (c) The corresponding imaginary part of the refractive index $n_i(x)$ following from the CI design principle for the real index distribution in (a), where gain is depicted in red an loss in green (we use these colors for all following figures). (d),(e) Scattering wave functions for the disordered potential region as a function of the gain strength, for the gain-only and gain/loss refractive index, respectively, for an incident plane wave with wavenumber $k_0 = 2\pi/0.1 = 62.8$. The CI wave can be clearly seen for the full gain/loss strength in (e). These and all following simulations of this chapter were performed by using the transfer-matrix method [31].

2.2 Resonance Width

A constant intensity interference pattern goes hand in hand with perfect transmission of the incident wave, whereas full transmission can also be achieved without a constant intensity pattern as we all know from a Fabry-Pérot interferometer. In this latter example, interference of multiply reflected rays between two highly reflecting mirrors (high Q-factor) leads to peaks in the transmission spectrum when the resonance condition

$$L = \frac{m\lambda}{2n} \tag{2.9}$$

is fulfilled, where λ is the vacuum wavelength of the incident wave, m an integer and L the length of the resonator with constant refractive index n. If the incident wavelength is changed just slightly, the phase relation between the back and forth propagating waves changes which leads to a significantly different interference pattern, thus leading to sharp transmission peaks. Even in Anderson localized systems, perfect transmission can be observed for certain wavelengths, but also here the resonance width is small. In the following, we want to investigate the resonance width of CI systems using a Fabry-Pérot-like system.

A resonance in the transmission spectrum $|t(k)|$ can be associated with a pole in the extended complex k-plane, where the width of the resonance is determined by the distance between the pole and the real k-axis. These poles can be calculated by using the effective Hamiltonian approach explained in [32]. In the aforementioned example of a Fabry-Pérot interferometer, an incident plane wave with a wavelength not fulfilling the resonance condition leads to a transmission amplitude less than 1 - perfect transmission with constant intensity can, however, be restored by adding the corresponding constant-intensity gain/loss distribution to the Fabry-Pérot system. The transition from the Hermitian system with low transmission to the constant-intensity system with perfect transmission is investigated by looking at the movement of the poles in the complex k-plane when gradually increasing the gain/loss strength. In the following simulations, we approximate the Fabry-Pérot interferometer by the real part of a CI refractive index distribution $n_r(x)$ that is derived from a generating function $W(x)$ with the shape of a super Gaussian, as can be seen in Fig. 2.2(a). Fig. 2.2(c) shows the absolute value of the transmission amplitude as a function of the incident wavenumber k, whereas in Fig. 2.2(e) we can see the transmission amplitude in the extended complex k-plane. As expected, we see sharp resonance peaks resulting from the poles in the complex k-plane. Adding the corresponding constant-intensity gain/loss distribution, see Fig. 2.2(b), the poles move to new positions, which are such that the transmission becomes $|t| = 1$ at the chosen wavenumber k_0, as can be seen in Fig. 2.2(d) and Fig. 2.2(f). Contrary to the Hermitian system, the resonance at k_0 is not a sharp peak any longer but rather a broad plateau, indicating that the emergence of constant-intensity waves is a phenomenon with an inherent frequency robustness.

Due to the fact that the transmission is close to 1 in a large window compared to the width of the transmission peaks in the Hermitian system, we can conclude that the constant intensity interference pattern does not come from the interference of multiple reflected rays. This assumption is supported by the following consideration: In the center of the potential region, i.e., between the two rising edges of the refractive index, the generating function $W(x)$ can be assumed to be constant which results in $n_r(x) = \text{const} = n_r$ and $n_i(x) = 0$, according to Eq. (2.8). The constant-intensity solution in this region is thus given by $\psi(x) = e^{jk_0 \int W(x')dx'} = e^{jk_0 n_r x}$, which is just a plane wave propagating to the right-hand side, i.e., there is no back reflected wave at all. Due to a missing back reflected wave, there is no interference, thus changing the incident wavelength does not change the intensity pattern significantly (like in a Hermitian Fabry-Pérot interferometer), which explains the stability of this phenomenon. In other words, the robustness of constant-intensity waves originates in the fact that each subpart of the entire scattering region already gives rise to constant-intensity rather than only all of them together.

Through the above we show that constant-intensity systems are stable, in the sense that a shift Δk of the incident wavenumber, i.e., $k = k_0 + \Delta k$, may still lead to a transmission close to unity, even when the same system without the constant-intensity gain/loss distribution shows a significant change in the transmission. One has to mention that gain/loss materials are dispersive, i.e., the amplifying/absorbing effect depends on the incident wavelength, whereas in our calculations we assumed that gain/loss is frequency independent, which is a valid assumption for a narrow frequency window.

Our results demonstrate that the constant-intensity solution inside the potential region shown in Fig. 2.2(b) is given by a plane wave propagating to the right-hand side. The counter propagating wave which exists in the Hermitian system is completely suppressed by adding the constant-intensity gain/loss part. In quantum mechanics, systems without back reflections, like the CI system at hand, are often described in the WKB-approximation. In the next section we show that this approximation is exact for all constant-intensity systems.

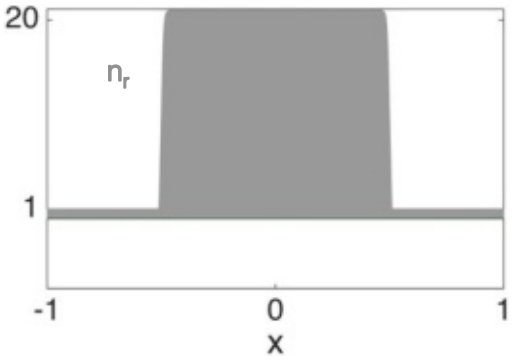

(a) System with the Hermitian part of the CI refractive index distribution that is derived from a super Gaussian shaped generating function $W(x) = 20e^{x^{100}}$ to simulate a Fabry-Pérot interferometer.

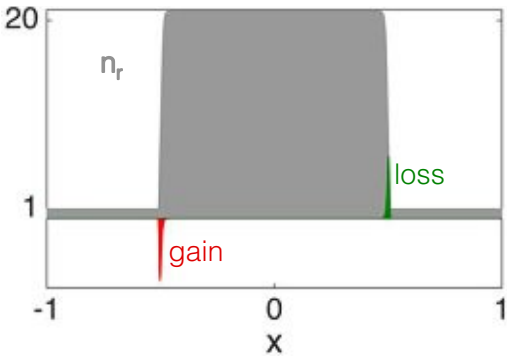

(b) System with the full CI refractive index distribution that is derived from a super Gaussian shaped generating function $W(x) = 20e^{x^{100}}$.

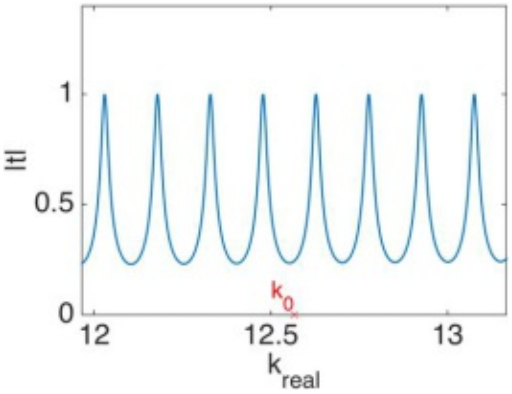

(c) Absolute value of the transmission as a function of the incident wavenumber k for the system shown in (a). Just like a Fabry-Pérot interferometer, the resonances appear when the resonance condition (2.9) is fulfilled.

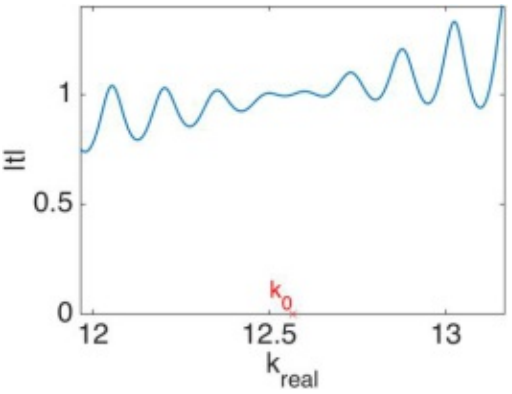

(d) Absolute value of the transmission as a function of the incident wavenumber k for the system shown in (b). Not only at $k_0 = 2\pi/0.5 = 12.57$ we have perfect transmission, but also in the vicinity of k_0 the transmission is close to 1.

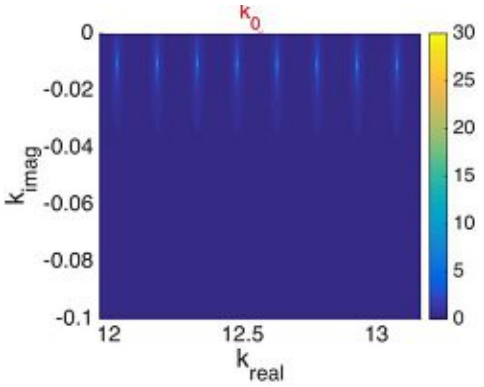

(e) Absolute value of the transmission (see color bar) in the complex k-plane for the system shown in (a). The resonances in (c) come from the singularities (bright spots) in the complex plane. (c) is a cut of this graphic at $k_{imag} = 0$.

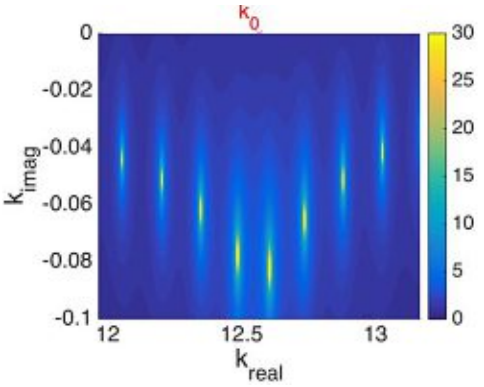

(f) Absolute value of the transmission (see color bar) in the complex k-plane for the system shown in (b). The singularities arrange themselves in such a way that the transmission becomes 1 at k_0. (d) is a cut of this graphic at $k_{imag} = 0$.

Figure 2.2

2.3 WKB-Approximation

In semiclassical mechanics, WKB-theory provides a good approximation for the wave function in systems where the potential $V(x)$ varies slowly compared to the de-Broglie-wavelength of the quantum particle. Inspired by the solution of a particle traveling in a constant potential $V(x) = V_0$, $\psi(x) = Ae^{\pm\frac{j}{\hbar}p_0 x}$, the first order WKB-approximation yields $\psi(x) = Ae^{\pm\frac{j}{\hbar}\int p(x')dx'}$, with A being a constant, $p(x) = \sqrt{2m(E-V_0)}$ the position-dependent momentum and E the energy of the particle. Higher order correction terms can be gained by expanding the WKB-ansatz in powers of $\hbar$. Using the mathematical equivalence of the stationary Schrödinger equation and the Helmholtz equation for scattering states, we now show that the WKB-approximation is exact for constant-intensity waves.

Making an ansatz for the wave function $\psi(x) = e^{jS(x)}$, where $S(x)$ is a complex function, and inserting it into the Helmholtz equation (2.2), yields

$$jS''(x) - S'^2(x) + k_0^2 n^2(x) = 0. \tag{2.10}$$

Eq. (2.10) is equivalent to the Helmholtz equation, since no approximation has been made so far. We expand the function $S(x)$ in powers of a small parameter δ,

$$S(x) = \frac{1}{\delta}\sum_{n=0}^{\infty}\delta^n S_n(x), \tag{2.11}$$

where in quantum mechanics δ would be replaced by $\hbar$. For a better readability, we skip the arguments of all variables with an obvious x-dependence. Inserting the WKB-ansatz (2.11) into Eq. (2.10), we get

$$\begin{aligned} &j\frac{1}{\delta}(S_0'' + \delta S_1'' + \delta^2 S_2'' + \delta^3 S_3'' + \dots) \\ &-\frac{1}{\delta^2}(S_0' + \delta S_1' + \delta^2 S_2' + \delta^3 S_3' + \dots)^2 + k_0^2 n^2 = 0. \end{aligned} \tag{2.12}$$

In a next step, we have to find out the asymptotic scaling of δ in terms of k_0. To leading order, Eq. (2.12) can be approximated by $j\frac{1}{\delta}(S_0'') - \frac{1}{\delta^2}(S_0')^2 - \frac{2}{\delta}S_0'S_1' + k_0^2 n^2 = 0$, where in the limit of $\delta \to 0$, the dominant balance is given by

$$\frac{1}{\delta^2}(S_0')^2 = k_0^2 n^2. \tag{2.13}$$

Thus, δ and k_0 are indirectly proportional to each other and we can set $\frac{1}{k_0} = \delta$. Considering the first four terms of the expansion and collecting terms with the same

power of k_0, we end up with

$$k_0^2 = \frac{1}{\delta^2}: \qquad n^2 - (S_0')^2 = 0 \tag{2.14}$$

$$k_0^1 = \frac{1}{\delta^1}: \qquad jS_0'' - 2S_0'S_1' = 0 \tag{2.15}$$

$$k_0^0 = \frac{1}{\delta^0}: \qquad jS_1'' - 2S_0'S_2' - (S_1')^2 = 0 \tag{2.16}$$

$$k_0^{-1} = \frac{1}{\delta^{-1}}: \qquad jS_2'' - 2S_0'S_3' - 2S_1'S_2' = 0. \tag{2.17}$$

From Eq. (2.15)-(2.17) we can see that if $S_m' = 0$, it follows that $S_{n>m}' = 0$ if $S_0' \neq 0$. So, if we demand that the first order approximation should be exact, we have to make sure that $S_1' = 0$. By assuming that the imaginary part of n^2 is proportional to $\frac{1}{k_0}$, it will move from Eq. (2.14) to Eq. (2.15), giving us the possibility to cancel the term jS_0'' in Eq. (2.15) by choosing $\mathrm{Im}(n^2) = -\frac{j}{k_0}S_0''$. As a result, Eq. (2.15) becomes $2S_0'S_1' = 0$, which is only fulfilled if $S_1' = 0$, since $S_0' \neq 0$. For a constant-intensity wave, $S(x)$ has to be real, so that Eq. (2.14) determines the real part of n^2, i.e., $\mathrm{Re}(n^2) = (S_0')^2$. We end up with $n^2 = (S_0')^2 - \frac{j}{k_0}S_0''$, which gives the constant-intensity refractive index (2.4) if we set $S_0' = W$. Since $S_{n>0}' = 0$ means that $S_{n>0} = \mathrm{const}$, one can choose them to be zero.

In this way we show that constant-intensity refractive indices are the direct consequence of demanding that a WKB-approximation is exact in non-Hermitian systems. The result is quite surprising, since the WKB-approximation for Hermitian systems is only valid when the refractive index varies slowly compared to the wavelength. The WKB-approximation for constant-intensity waves, however, is valid even when the real part of the refractive index is highly oscillatory, provided of course that the corresponding gain/loss distribution is added. In the same way as the WKB-approximation is exact in Hermitian systems with constant refractive index $n(x) = n_0$, we show that exact WKB-approximations can exist in non-Hermitian systems if the refractive index supports constant-intensity waves.

Looking carefully at the construction of constant-intensity refractive indices (2.4) which involves the square and the derivative of the function $W(x)$, one can assume that constant-intensity waves are related to supersymmetric quantum mechanics (SUSY QM), since these two elements (square and derivative of a function) are essential in the construction of so-called partner potentials. In the next section we present the connection between these two topics.

2.4 Connection to Supersymmetry

Supersymmetric quantum mechanics involves pairs of Hamiltonians, so-called partner Hamiltonians, with corresponding partner potentials. These partner Hamiltonians share the same set of eigenvalues, except the ground state, and are both

connected by a so-called superpotential. If, however, both partner potentials have the same ground state energy, then SUSY is said to be broken [33]. Originally developed in the context of quantum field theory, some aspects of SUSY have already been transferred to optics, where SUSY can establish close relationships between seemingly different dielectric structures [34, 35].

In the following chapter we, show that in the framework of SUSY quantum mechanics, CI systems can be described by Hamiltonians that can be derived from a specific class of superpotentials. We start with the Helmholtz equation and use SUSY formalism to find its solution as a function of the superpotential. By demanding constant intensity of the solution, we find constraints for the superpotential.

For the following derivation, quantities that are related to the original constant-intensity refractive index are labeled with a subscript (1), whereas the corresponding supersymmetric quantities (partner potential and partner Hamiltonian) are labelled with (2). For a better readability, we skip the arguments of all variables with an obvious x-dependence.

Rewriting the Helmholtz equation

$$\left(\frac{d^2}{dx^2} + k_0^2 n_{(1)}^2\right)\psi_{(1)} = 0 \tag{2.18}$$

as a Schrödinger equation

$$\left(-\frac{1}{2}\frac{d^2}{dx^2} + V_{(1)}\right)\psi_{(1)} = H_{(1)}\psi_{(1)} = E_{(1)}\psi_{(1)}, \tag{2.19}$$

with

$$H_{(1)} = -\frac{1}{2}\frac{d^2}{dx^2} + V_{(1)}, \tag{2.20}$$

$$V_{(1)} = \left(1 - n_{(1)}^2\right)\frac{k_0^2}{2}, \tag{2.21}$$

and eigenenergy $E_{(1)} = \frac{k_0^2}{2}$, one can factorize $H_{(1)} - E_{(1)} = BA$, in analogy to Eq. (3)-(4) in Ref. [33] , with

$$A = \frac{1}{\sqrt{2}}\frac{d}{dx} + \Omega(x), \tag{2.22}$$

$$B = -\frac{1}{\sqrt{2}}\frac{d}{dx} + \Omega(x), \tag{2.23}$$

where $\Omega(x)$ is the (complex) superpotential. The potential $V_{(1)}$ can be expressed in terms of the superpotential as follows

$$V_{(1)} = \Omega^2 - \frac{1}{\sqrt{2}}\Omega' + \frac{k_0^2}{2}. \tag{2.24}$$

For Hermitian systems, i.e., real potentials (or refractive indices) it would follow that $\Omega \in \mathbb{R}$ and $B = A^\dagger$. Defining a partner Hamiltonian as $H_{(2)} - E_{(1)} = AB$, one ends up with the partner potential

$$V_{(2)} = \Omega^2 + \frac{1}{\sqrt{2}}\Omega' + \frac{k_0^2}{2}. \tag{2.25}$$

From

$$(H_{(1)} - E_{(1)})\psi_{(1)} = BA\psi_{(1)} = 0 \tag{2.26}$$

follows that A annihilates $\psi_{(1)}$, i.e.,

$$A\psi_{(1)} = \left(\frac{1}{\sqrt{2}}\frac{d}{dx} + \Omega\right)\psi_{(1)} = 0, \tag{2.27}$$

which can be used to calculate $\psi_{(1)}$,

$$\psi_{(1)} = e^{-\sqrt{2}\int \Omega(x')dx'}. \tag{2.28}$$

A scattering state with a constant intensity can be obtained by choosing Ω purely imaginary. Taking $\Omega = j\frac{k_0}{\sqrt{2}}W$ with $W \in \mathbb{R}$, we end up with the well-known CI solution

$$\psi^{(1)} = e^{-jk_0\int W(x')dx'}, \tag{2.29}$$

with potential

$$V_{(1)} = -\frac{k_0^2}{2}W^2 - j\frac{k_0}{2}W' + \frac{k_0^2}{2} = \left(1 - n_{(1)}^2\right)\frac{k_0^2}{2}, \tag{2.30}$$

from which the refractive index $n_{(1)}$ can be calculated,

$$n_{(1)} = \sqrt{W^2 + \frac{j}{k_0}W'}. \tag{2.31}$$

The partner potential $V_{(2)}$ reads as follows,

$$V_{(2)} = -\frac{k_0^2}{2}W^2 + j\frac{k_0}{2}W' + \frac{k_0^2}{2} = \left(1 - n_{(2)}^2\right)\frac{k_0^2}{2}, \tag{2.32}$$

with corresponding refractive index

$$n_{(2)} = \sqrt{W^2 - \frac{j}{k_0}W'}, \tag{2.33}$$

and corresponding CI solution

$$\psi_{(2)} = e^{jk_0\int W(x')dx'}, \tag{2.34}$$

which is equivalent to the presented results in section 2.1. Solution (2.34) represents a wave traveling from the left-hand side to the right-hand side of the system with refractive index (2.33), whereas Eq. (2.29) represents a wave traveling from the right to the left with complex conjugate refractive index. These two situations can be interpreted as the time-reversed processes of each other, since the time-reversal operator $\mathcal{T}$ performs a complex conjugation $j \to -j$, i.e., it turns gain into loss (and loss into gain) and changes the side of injection.

In summary, we show in this section that constant-intensity waves can alternatively be derived from SUSY QM by demanding that the superpotential has to be purely imaginary. This superpotential is related to the generating function $W(x)$ just by a multiplicative factor and leads to two partner potentials (refractive indices) supporting constant-intensity waves for either side of injection. These interesting observations and their possible consequences will be the subject of further investigations. Apparently, symmetries play an important role in constant-intensity systems, therefore we investigate the connection to $\mathcal{PT}$-symmetry in the next section.

2.5 Connection to $\mathcal{PT}$-Symmetry

We all know from quantum mechanics that the Hamiltonian has to be a Hermitian operator to ensure that its eigenvalues are real. However, Bender et al. pointed out that there is a whole class of non-Hermitian but "$\mathcal{PT}$-symmetric" Hamiltonians that possesses real spectra as well [20, 21]. The $\mathcal{PT}$-operator is a combination of the parity-operator $\mathcal{P}$, flipping the spatial coordinate $x \to -x$, and the time-reversal operator $\mathcal{T}$ that performs a complex conjugation $j \to -j$, i.e., turns gain into loss (and loss into gain) and changes the side of injection. A Hamiltonian H is called $\mathcal{PT}$-symmetric if the commutator $[\mathcal{PT}, H] = 0$ and furthermore a complex refractive index $n(x) = n_r(x) + jn_i(x)$ is called $\mathcal{PT}$-symmetric if the condition $\mathcal{PT}n(x) = n^*(-x) = n(x)$ is satisfied, i.e., if the real part of the refractive index is an even function, $n_r(x) = n_r(-x)$, and the imaginary part an odd function, $n_i(x) = -n_i(-x)$, of the spatial coordinate x. In the following, we investigate the connection between $\mathcal{PT}$-symmetry and CI waves.

Given an arbitrary generating function $W(x)$ fulfilling the boundary conditions, one can calculate the corresponding CI refractive index

$$n(x) = \sqrt{W^2(x) - \frac{j}{k_0}W'(x)}. \tag{2.35}$$

One can start from the given generating function $W(x)$ and find another generating function $\mathcal{P}W(x) = W(-x)$, that also leads to a CI wave with refractive index

$$\tilde{n}(x) = \sqrt{W^2(-x) - \frac{j}{k_0}W'(-x)}. \tag{2.36}$$

One can show that the refractive index $\tilde{n}(x)$ can also be obtained by applying the $\mathcal{PT}$-operator on the constant-intensity refractive index $n(x)$. Hence, starting from an arbitrary constant-intensity refractive index $n(x)$, one can easily find another constant-intensity refractive index $\tilde{n}(x)$ by

$$\tilde{n}(x) = \mathcal{PT}n(x). \tag{2.37}$$

Both refractive indices, $\tilde{n}(x)$ and $n(x)$, lead to a constant-intensity wave for the same side of injection. If $W(x)$ is an even function, i.e., if $n(x)$ is $\mathcal{PT}$-symmetric, $n(x)$ and $\tilde{n}(x)$ coincide. The fact that $\tilde{n}(x)$ and $n(x)$ both lead to constant-intensity waves brings up the question if constant-intensity systems have a strong connection to $\mathcal{PT}$-symmetry, which is discussed in the following.

Since the integral of $W(x)$ is the same as the integral of $W(-x)$ over the entire scattering region, both refractive indices, $n(x)$ and $\tilde{n}(x)$, lead to the same transmission amplitudes $t = e^{jk_0\int_{-L}^{L} W(x')dx'} = \tilde{t} = e^{jk_0\int_{-L}^{L} W(-x')dx'}$. Thus, $n(x)$ and $\tilde{n}(x)$ are indistinguishable in the transmission amplitude. Whereas this result is trivial for $\mathcal{PT}$-symmetric systems, where $n(x)$ and $\tilde{n}(x)$ coincide, this connection is surprising for non-$\mathcal{PT}$-symmetric systems and stems from the constant-intensity nature of the underlying refractive index.

Another connection to $\mathcal{PT}$-symmetry can be found by looking at the eigenvalues $\lambda_{1,2}$ of the scattering matrix S of CI systems. Since time-reversal symmetry is not broken, it follows that $t_r = t_l = t = e^{jk_0\int_{-L}^{L} W(x')dx'}$. Calculating the determinant of the scattering matrix

$$\det(S) = \det\begin{pmatrix} r_l & t \\ t & r_r \end{pmatrix} = \det\begin{pmatrix} 0 & e^{jk_0\int_{-L}^{L} W(x')dx'} \\ e^{jk_0\int_{-L}^{L} W(x')dx'} & r_r \end{pmatrix} = -e^{2jk_0\int_{-L}^{L} W(x')dx'}, \tag{2.38}$$

and using the relation $\lambda_1\lambda_2 = \det(S)$, one can show that the absolute value of the eigenvalues are related to each other by $|\lambda_1| = \frac{1}{|\lambda_2|}$, which is valid in the so-called broken and unbroken phase of any $\mathcal{PT}$-symmetric system [36]. If we calculate the eigenvalues $\tilde{\lambda}_{1,2}$ of the scatting matrix $\tilde{S}$, which is defined as

$$\tilde{S} = \begin{pmatrix} t & r_r \\ r_l & t \end{pmatrix} = \begin{pmatrix} e^{jk_0\int_{-L}^{L} W(x')dx'} & r_r \\ 0 & e^{jk_0\int_{-L}^{L} W(x')dx'} \end{pmatrix}, \tag{2.39}$$

we end up with $\tilde{\lambda}_{1,2} = e^{jk_0\int_{-L}^{L} W(x')dx'}$, i.e., the eigenvalues are degenerate. Here we want to mention that the definition of the scattering matrix as in Eq. (2.39) is not conventional, however, it shows some interesting features. One can show that also the eigenvectors $\vec{\nu}_{1,2}$ of $\tilde{S}$ are the same, so that eigenvalues and eigenstates have coalesced. According to the definition of the scattering matrix in Eq. (2.39), constant-intensity waves thus occur at so-called exceptional points of $\tilde{S}$. Furthermore, the eigenvalues follow the relation $|\tilde{\lambda}_{1,2}| = \frac{1}{|\tilde{\lambda}_{1,2}|}$ which is valid in the so-called

unbroken phase of $\mathcal{PT}$-symmetric systems and imposes that the eigenvalues are unimodular. The connection between CI waves and exceptional points is still being investigated and may lead to new insights into non-Hermitian physics.

These similarities between CI systems and $\mathcal{PT}$-symmetric systems can come from the fact that in CI systems the average gain/loss is zero in terms of the dielectric function $\epsilon(x)$, since $\int_{-L}^{L} \mathrm{Im}[\epsilon(x)]dx = \int_{-L}^{L} \frac{dW(x)}{dx} = W(L) - W(-L) = 0$. Due to the fact that the intensity of the wave is constant in the whole scattering region, the wave is equally distributed in gain regions as in loss regions and so the net amplification/attenuation is zero. In terms of the refractive index, however, the evaluation of the integral $\int_{-L}^{L} n_i(x)dx$ depends on the symmetry of $W(x)$.

Due to the fact that the phase of constant-intensity waves is given as the integral over a function $W(x)$, one can create a scattering state with a predetermined phase profile by fixing $W(x)$. This fact can be used to hide the information about the scattering region by delicately choosing $W(x)$, as presented in the next section.

2.6 Unidirectional Invisibility

Another interesting feature of CI waves is the connection to the well-known phenomenon of "unidirectional invisibility" which was predicted in 2011 by Zin Lin et al. [22] and has already been verified experimentally [37, 38]. The complex transmission amplitude of a unidirectionally invisible material is indistinguishable from the transmission amplitude of a uniform material and furthermore, the reflection from one end is diminished. Both conditions are necessary to evade detectability.

The first potential that was proposed for the realization of this interesting effect was a periodic refractive index distribution [22],

$$n(x) = n_0 + n_1 \cos(2\beta x) + j n_2 \sin(2\beta x), \tag{2.40}$$

which was stated to be unidirectionally invisible when the wavenumber of the incident wave is equal to the modulation frequency of the refractive index, $k = \beta$ (Bragg point), and when $n_1 = n_2$. The simulations were performed with the parameters $n_0 = 1$ and $n_1 = n_2 = 10^{-3}$. Since sine and cosine can be negative, the refractive index in Eq. (2.40) can be smaller than 1, which is unphysical. Since, however, n_1 and n_2 are very small, the authors neglected this issue (the authors did not comment about that in the paper).

In this section we investigate the invisibility of CI refractive indices and show that the unidirectionally invisible refractive index that was used in Ref. [22], Eq. (2.40), is just one example of this subclass. The specific form of constant-intensity waves, $\psi(x) = e^{jk_0 \int W(x')dx'}$, gives us the possibility to construct a non-constant refractive index $n(x)$ featuring gain and loss that enables a wave to traverse the scattering region as if there were no index variations, i.e., like propagating in a uniform material. This concept of invisibility works for arbitrary generating functions of the

form

$$W(x) = n_0 + f(x), \tag{2.41}$$

where $f(x)$ is a function satisfying $\int_{-L}^{L} f(x')dx' = 0$ and $n_0 \geq 1$ is an "offset" which ensures that $n_r(x) \geq 1$, since $f(x)$ can be negative. To avoid reflections at the beginning and at the end of the potential region, the free space before and after the potential region has to have a constant refractive index n_0, thus the boundary conditions for $W(x)$ change to $W(-L) = W(L) = n_0$. The term "unidirectional" comes from the fact that if we inject a wave from the opposite site, there is no constant-intensity wave and in this way hiding the index variations would not work. However, if we complex conjugate $n(x)$, i.e., turn gain into loss and vice versa, one can get a constant-intensity wave for injection from the opposite site, as discussed in section 2.4. The transmission amplitude of a wave traveling through a constant-intensity refractive index of length $2L$ with generating function (2.41) takes the form

$$t = e^{jk_0 \int_{-L}^{L} W(x')dx'} = e^{2jk_0 n_0 L} e^{jk_0 \int_{-L}^{L} f(x')dx'} = e^{2jk_0 n_0 L}. \tag{2.42}$$

Since the transmission amplitude of a wave traveling through a uniform material with $n(x) = n_0$ is the same as (2.42), one cannot distinguish between these two systems by looking at the phase of the transmission amplitude at only one frequency. However, if we change the frequency and look at the frequency dependence of the transmission phase (see time-delay), systems with a non-uniform refractive index will generally lead to a different frequency dependence than uniform materials, thus giving us the opportunity to detect them. Since constant-intensity waves stay to a great extent constant in a rather broad frequency range around k_0 (the wavenumber that was used to construct $n(x)$), as shown in section 2.2, one can assume that the wave behaves like $\psi(x) = e^{jk \int W(x')dx'}$ around k_0. Calculating the time-delay $\tau = -jt^{-1}\frac{dt}{d\omega}$ of the CI wave gives

$$\tau = \frac{|\int_{-L}^{L} W(x)\,\mathrm{d}x|}{c} = \frac{2n_0 L}{c}, \tag{2.43}$$

for CI systems with generating functions (2.41). Thus, we show that also the frequency dependence in a certain range around k_0 is the same as for the propagation through a uniform material (namely constant) and therefore CI refractive indices with generating functions (2.41) can be considered unidirectionally invisible. Here we want to emphasize that constant-intensity waves are not unidirectionally invisible *in general*, since the integral over the generating function $W(x)$ does not necessarily yield the phase of a wave traveling through a uniform material.

We want to show now, that the previously introduced and periodic refractive index shown in Eq. (2.40) can be derived from a CI refractive index with generating function

$$W(x) = n_0 + n_1 \cos(2\beta x) \tag{2.44}$$

in the limit of small variations of the refractive index ($n_1, n_2 \ll 1$). The corresponding CI refractive index yields

$$\begin{aligned} n(x) &= \sqrt{W^2(x) - \frac{j}{k_0}\frac{dW(x)}{dx}} \\ &= n_0\sqrt{1 + \frac{n_1^2}{n_0^2}\cos^2(2\beta x) + \frac{2n_1}{n_0}\cos(2\beta x) + j\frac{2\beta n_1}{k_0 n_0^2}\sin(2\beta x)}. \end{aligned} \tag{2.45}$$

Neglecting the term proportional to $n_1^2 \propto 10^{-6}$ in Eq. (2.45) and assuming $k_0 = \beta$, we end up with $n(x) = n_0\sqrt{1 + 2n_1/n_0\cos(2\beta x) + 2jn_1/n_0^2\sin(2\beta x)}$. Since n_1 is small compared to n_0, one can expand the square root $\sqrt{1+x} = 1 + \frac{x}{2} + ...$ for small $x = \frac{2n_1}{n_0}[\cos(2\beta x) + j\sin(2\beta x)]$ and keep only the first two terms of the expansion. We end up with

$$n(x) = n_0 + n_1\cos(2\beta x) + j\frac{n_1}{n_0}\sin(2\beta x), \tag{2.46}$$

which is identical to Eq. (2.40) if $n_0 = 1$ and $n_1 = n_2$. In the limit of small variations, (2.40) is indeed a constant-intensity refractive index. Thus, unidirectional invisibility does not stem from the $\mathcal{PT}$-symmetry of the structure, but from the constant-intensity form of the wave function.

In order to prove our predictions also numerically, we perform the same simulations that were reported in Ref. [22] with (2.40) but now with the constant-intensity refractive index (2.45). In Fig. 2.3(a) we can see the transmittance $T = |t|^2$, the reflectance to the left $R_l = |r_l|^2$ and the reflectance to the right $R_r = |r_r|^2$ as a function of the detuning $\delta = \beta - k$ for a system with refractive index (2.45) compared with the same quantities in the corresponding Hermitian system, i.e., without gain and loss. In the non-Hermitian system, the transmittance T is close to unity over the entire interval, whereas in the Hermitian system the transmittance T drops significantly at $\delta = 0$ because of Bragg reflection. Additionally, the reflectance to the left R_l stays close to zero in the non-Hermitian system and increases at the Bragg point in the Hermitian system. In the non-Hermitian system, the phase of the transmission amplitude ϕ_t and its derivative, the time-delay $\tau = \frac{d\phi_t}{dk}$ (we set the speed of light $c \equiv 1$), behave as if the system was uniform, whereas those quantities show huge variations in the Hermitian system, as can be seen in Fig. 2.3(b) and 2.3(c). The behavior of the observed quantities leads us to the conclusion that the system is invisible. Fig. 2.3(d) shows that both refractive indices, (2.45) and (2.40) lead to the same scattering amplitudes in the above mentioned approach for small index variations, thus proving our prediction that the unidirectionally invisible refractive index of Ref. [22] is in fact a constant-intensity refractive index.

One important feature has to be pointed out in the following: Unlike the refractive index in Eq. (2.45), general invisible CI refractive indices do not have to be periodic, which is demonstrated with an example. As mentioned above, the generating function for unidirectionally invisible refractive indices has to be of the form

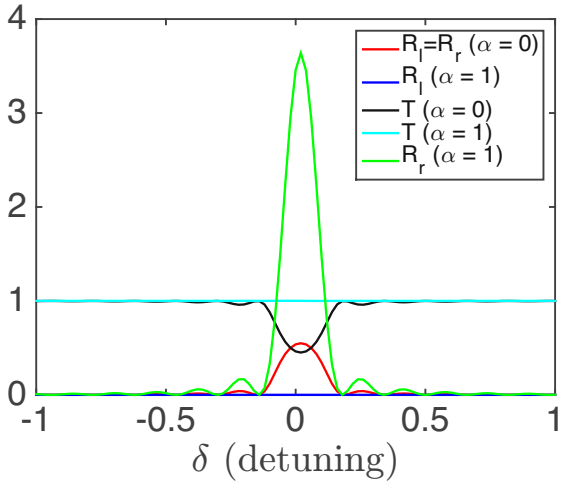

(a) Transmittance $T = |t|^2$ and reflectance $R_{r,l} = |r_{r,l}|^2$ (to the left and right) of a scattering system with CI refractive index (2.45) as a function of the detuning $\delta = \beta - k$ for the Hermitian case ($\alpha = 0$) and the non-Hermitian case ($\alpha = 1$). In the non-Hermitian system, the transmittance is exactly 1 and the reflectance to the left is exactly 0 at the Bragg point $\beta = k = k_0$, which corresponds to the constant-intensity point. R_r is enhanced at the Bragg point. T and R_l stay almost constant in the entire interval. In the Hermitian system, the transmittance decreases significantly at the Bragg point $\beta = k = k_0$.

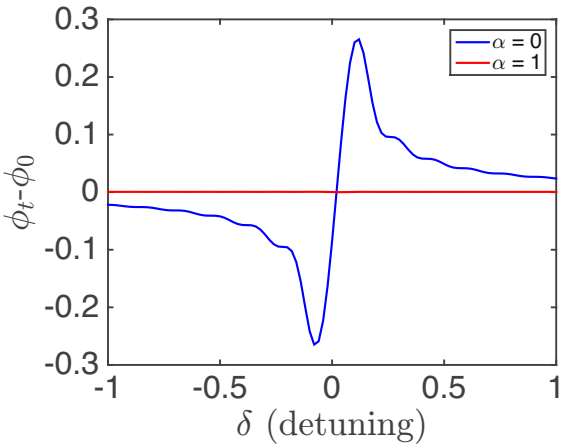

(b) Phase of the transmission amplitude ϕ_t minus phase that the wave would accumulate in a uniform material $\phi_0 = 2Lk_0n_0$ for the Hermitian and non-Hermitian case as a function of δ. For the non-Hermitian case, this value is zero in the entire interval, which is essential to call a system invisible.

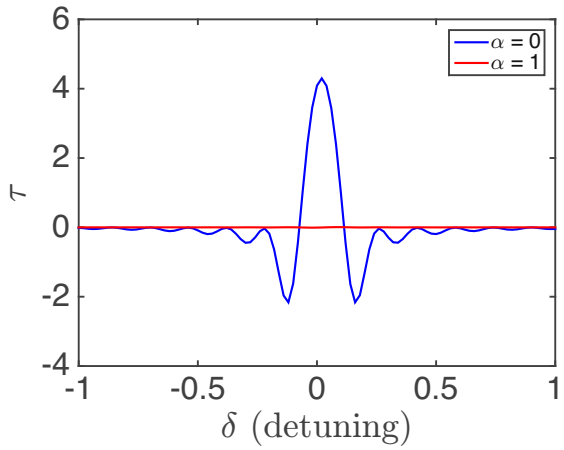

(c) Time-delay $\tau = \frac{d(\phi_t - \phi_0)}{dk}$ as a function of the detuning δ. Compared to the Hermitian system, the non-Hermitian system is invisible.

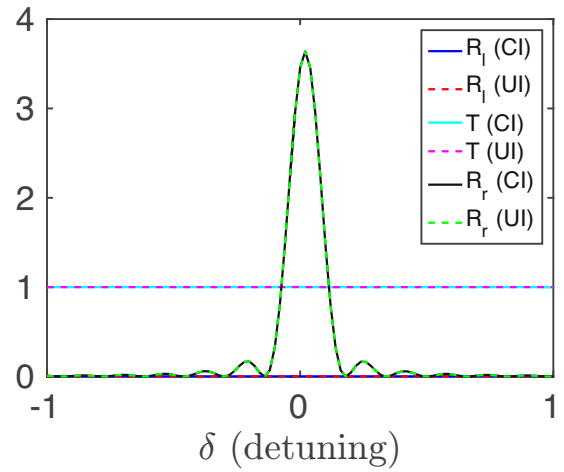

(d) Scattering amplitudes of the system with constant-intensity (CI) refractive index (2.45) compared to the system with unidirectionally invisible (UI) refractive index (2.40). As predicted, the systems are indistinguishable.

Figure 2.3: Parameters of the CI refractive index in Eq. (2.45): $n_0 = 1$, $n_1 = 10^{-3}$; $\beta = k_0 = 100$; System length $2L = L_1 + L_2$ with $L_1 = 6.25\pi$ of index variations and $L_2 = \pi$ of free propagation. Parameters of the unidirectionally invisibility refractive index (2.40): $n_1 = n_2$. All the other values are the same as for the CI refractive index. The relative width of the scan interval of this calculation is $\Delta k/k_0 = 2/100 = 0.02$.

(2.41). For $f(x)$ we took n (n is an even number) randomly distributed identical non-overlapping Gaussian functions, where half of them have a positive sign and the other half has a negative sign in order to assure that the integral of $f(x)$ gives zero. The resulting refractive index is shown in Fig. 2.4(a), whereas the corresponding scattering amplitudes, the phase of the transmission amplitude ϕ_t and the time-delay τ are shown in Fig. 2.4(b)-(d) as a function of the detuning $\delta = k_0 - k$. The transmission phase as well as the time-delay show strong variations as a function of the detuning in the Hermitian system compared to the non-Hermitian system, indicating that the non-Hermitian (constant-intensity) system can be considered invisible.

In this section we show that constant-intensity systems can be unidirectionally invisible by choosing the generating function of the form (2.41) and thus introducing a whole new class of invisible refractive indices. Not only the transmission phase, but also the phase derivative (time-delay) within a certain frequency range is indistinguishable from the corresponding quantities of a wave traveling through a uniform system. The connection to an already known unidirectionally invisible refractive index (2.40), which is stated as $\mathcal{PT}$-symmetric and periodic, is drawn. However, we show in the next subsection that there are some subtleties that have to be considered when using invisible $\mathcal{PT}$-symmetric refractive indices.

2.6.1 $\mathcal{PT}$-Symmetry and Unidirectional Invisibility

Unidirectional invisibility is claimed to be a consequence of the $\mathcal{PT}$-symmetric nature of the refractive index distribution (2.40) of Ref. [22], however, in the previous section we show that unidirectional invisibility can also be realized in non-$\mathcal{PT}$-symmetric systems. Now we want to go a step further and show that the refractive index (2.40), that is claimed to be $\mathcal{PT}$-symmetric *and* unidirectionally invisible, *cannot* possess both properties simultaneously.

As already mentioned before, a complex refractive index $n(x) = n_r(x) + jn_i(x)$ is called $\mathcal{PT}$-symmetric if the condition $n^*(-x) = n(x)$ is satisfied, i.e., if the real part of the refractive index is an even function, $n_r(x) = n_r(-x)$, and the imaginary part an odd function, $n_i(x) = -n_i(-x)$, of the spatial coordinate x. Looking at the equations connecting $n_r(x)$ and $n_i(x)$ of the constant-intensity refractive index with the generating function $W(x)$ in Eq. (2.8), one can see that the parity of $n_r(x)$ is determined by the parity of $W(x)$, e.g., if $W(x)$ is an even function, $n_r(x)$ is an even function as well (if $W(x)$ is an odd function, $n_r(x)$ is not necessarily an odd function). As we show in the last chapter, one condition for an invisible CI refractive index is that $W(x) = n_0 + f(x)$ with $\int_{-L}^{L} f(x')dx' = 0$. For periodic generating functions, this is only possible if $f(x)$ is an odd function with respect to the center of the potential region, from which follows that $n_r(x)$ is not an even function and in this way $n(x)$ is not $\mathcal{PT}$-symmetric. We illustrate this issue by showing a specific system: Fig. 2.5 shows two fractions of a periodic constant-

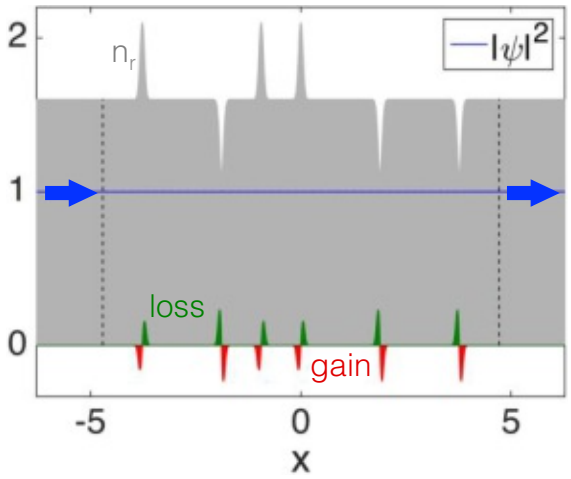

(a) Constant-intensity refractive index that features unidirectional invisibility. The refractive index was constructed with a generating function of the form (2.41), where $f(x)$ consists of identical non-overlapping Gaussian functions, where half of them have a positive sign and the other half has a negative sign. One has to add an "offset" $n_0 = 1.6$ so that $n_r(x) \geq 1$. The intensity of the wave function with wavenumber $k = k_0$ is shown in blue (constant-intensity point).

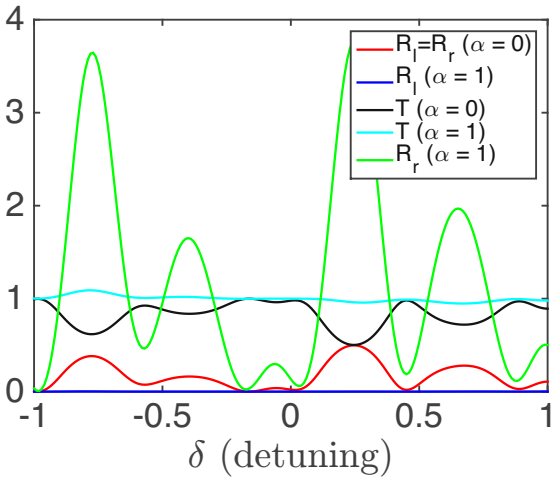

(b) Transmittance $T = |t|^2$ and reflectance $R_{r,l} = |r_{r,l}|^2$ (to the left and right) of a scattering system with the constant-intensity refractive index shown in (a) as a function of the detuning $\delta = k_0 - k$ for the Hermitian case ($\alpha = 0$) and the non-Hermitian case ($\alpha = 1$). In the non-Hermitian system, the transmittance is exactly 1 at $k_0 = k$ and the reflectance to the left is exactly 0, which corresponds to the constant-intensity point. T and R_l stay almost constant in the entire interval contrary to the Hermitian case.

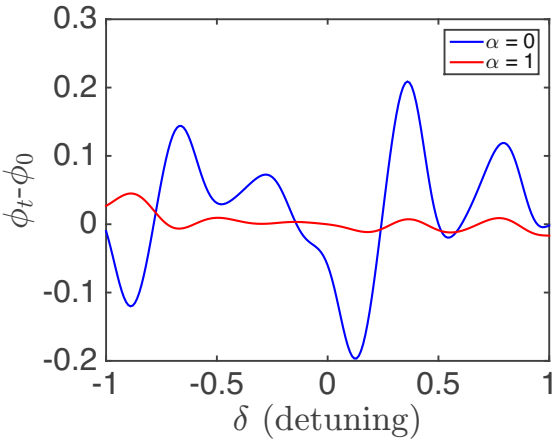

(c) Phase of transmission amplitude ϕ_t minus phase that the wave would accumulate in a uniform material $\phi_0 = 2Lk_0n_0$ for the Hermitian and non-Hermitian case as a function of the detuning δ. The value is almost zero in the entire interval for the non-Hermitian case, which is essential to call a system invisible.

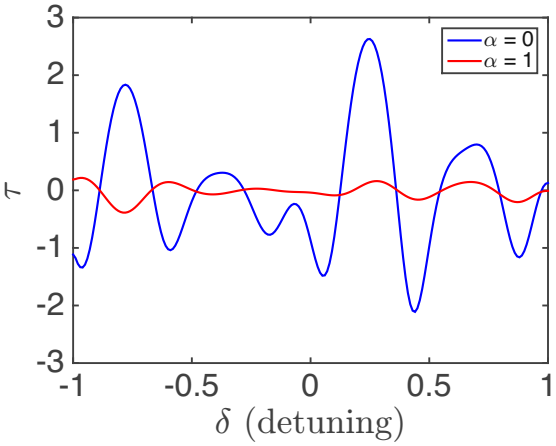

(d) Time-delay $\tau = \frac{d(\phi_t - \phi_0)}{dk}$ as a function of the detuning δ. Compared to the Hermitian system, the non-Hermitian system is invisible.

Figure 2.4: Parameters: $k_0 = 10$; System length $2L = L_1 + L_2$ with $L_1 = 3\pi$ of index variations and $L_2 = \pi$ of free propagation. Please note that the relative width of the scan interval in this system ($\Delta k/k_0 = 2/10 = 0.2$) is significantly larger than in the system shown in Fig. 2.3 ($\Delta k/k_0 = 0.02$) which explains the deviations from perfect invisibility at the ends of the interval.

intensity refractive index derived from the same generating function (2.44), where the first system, Fig. 2.5(a), has the length of half a cosine curve, whereas the second system, Fig. 2.5(b), consists of a full cycle. As a result, one of the systems is $\mathcal{PT}$-symmetric but not invisible and the other one is not $\mathcal{PT}$-symmetric but invisible, since only for one system the integral over $f(x)$ vanishes. Due to the fact that the unidirectionally invisible refractive index (2.40) of Ref. [22] can be derived from the CI refractive index with generating function (2.44) in the limit of small index variations ($n_1, n_2 \ll 1$), as shown in the previous section, all the statements concerning the CI refractive index do also apply to (2.40). Hence, the system can be either invisible *or* $\mathcal{PT}$-symmetric, but not both as stated in the reference. Probably the reason why this fact was overlooked so far is that the system in Ref. [22] is large compared to the wavelength and compared to the modulation frequency of the refractive index, such that one additional half-cycle of the refractive index (which decides if the system is $\mathcal{PT}$-symmetric or not) has almost no effect. But if we go to much smaller systems like in Fig. 2.5, the difference becomes, indeed, crucial.

In this subsection we show that for *periodic* generating functions, $\mathcal{PT}$-symmetry and invisibility cannot be fulfilled simultaneously, however, when going beyond periodic potentials invisible $\mathcal{PT}$-symmetric systems *can* be realized.

In the next section we show that we can generalize the concept of constant-intensity refractive indices to a much larger class of reflectionless refractive indices by allowing complex-valued generating functions $W(x)$ and show, that constant-intensity waves can be seen as a special case of these reflectionless refractive indices.

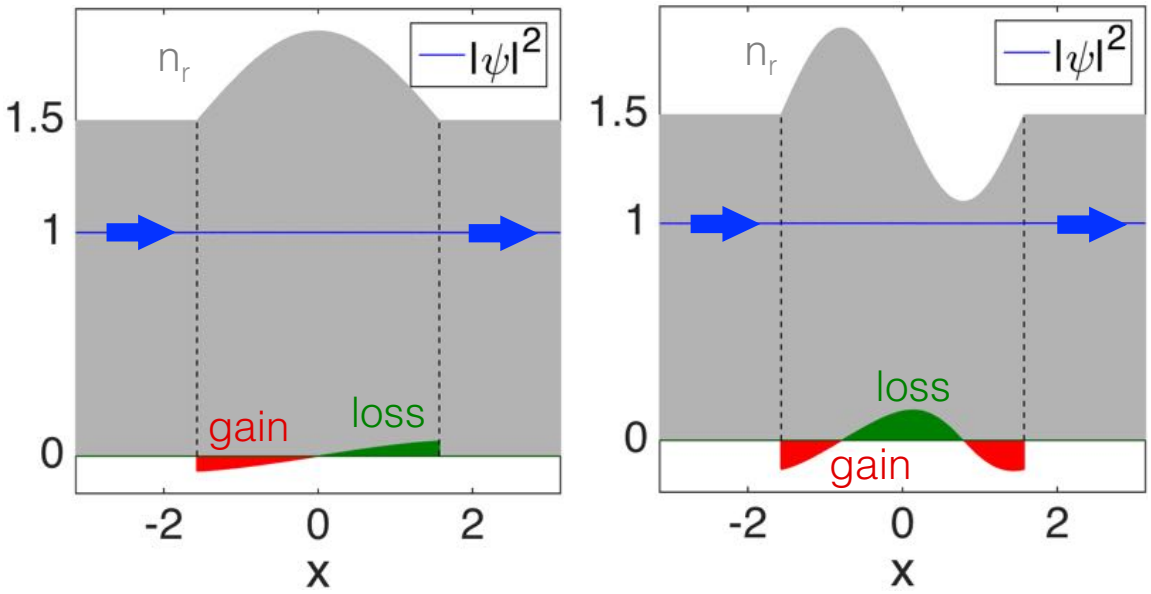

(a) Constant-intensity refractive index with generating function $W(x) = n_0 + n_1 \cos(2\beta x)$, where the length of the scattering region is half a cosine curve ($\beta = 0.5$). Obviously, this system is $\mathcal{PT}$-symmetric but not invisible, since the integral of $W(x)$ over half of a cosine cycle is not zero. Numerical results: $\phi_t - \phi_0 = -1.675$, where ϕ_t is the phase of the transmission amplitude and ϕ_0 is the phase of a wave traveling through a system without index modulations, $\phi_0 = 2k_0 n_0 L$.

(b) Constant-intensity refractive index with generating function $W(x) = n_0 + n_1 \cos(2\beta x)$, where the length of the scattering region is one full cosine curve ($\beta = 1$).This system is not $\mathcal{PT}$-symmetric but invisible, since the integral of $W(x)$ over one cosine cycle is zero. Numerical results: $\phi_t - \phi_0 = 1.514 \times 10^{-7}$, where ϕ_t is the phase of the transmission amplitude and ϕ_0 is the phase of a wave traveling through the system without index modulations, $\phi_0 = 2k_0 n_0 L$.

Figure 2.5: Two constant-intensity refractive indices with the same periodic generating function $W(x) = n_0 + n_1 \cos(2\beta x)$ with $n_0 = 1.5$ and $n_1 = 0.4$. Both systems have the smallest possible periodicity for showing the crucial difference. The physics would not change if we add multiples of full cosine cycles to the systems. Gain/loss is multiplied by a factor of 50 for a better visibility. In both system one can see the intensity of the wave function (blue) for an incident plane wave with $k_0 = 100$.

2.7 Wave Design

Since $W(x)$ determines the local phase of the scattering state, one can use the concept of constant-intensity waves to create a refractive index that leads to a wave function with a desired phase profile. Now we want to go a step further and try to additionally manipulate the amplitude of the wave as a function of the position. The goal of this chapter is to show how one can create a complex refractive index such that the amplitude and the phase of the scattering state can be manipulated arbitrarily for each value of the spatial coordinate x.

The derivation of the CI solution with corresponding refractive index in section 2.1 can be done in the same way with a complex generating function $W(x) = W_r(x) + jW_i(x)$, leading to the solution $\psi(x) = e^{jk_0 \int W_r(x')dx'} e^{-k_0 \int W_i(x')dx'}$, where the first part can be seen as the phase and the second part as the amplitude of the wave. Using the relations

$$W_i(x) = -\frac{1}{k_0}\frac{d}{dx}\ln[g(x)], \tag{2.47}$$

$$W_r(x) = n_0 + \frac{1}{k_0}\frac{d}{dx}h(x), \tag{2.48}$$

one can rewrite the wave function as

$$\psi(x) = g(x)e^{jh(x)}e^{jk_0 n_0 x}, \tag{2.49}$$

where $g(x)$ and $f(x)$ are real functions representing the amplitude and the additional phase profile (in addition to the phase that the wave would accumulate in a uniform material with refractive index n_0, $\phi_0(x) = k_0 n_0 x$), respectively. In all previous calculations we implicitly assume $n_0 = 1$. The refractive index supporting the scattering state (2.49) can be calculated straightforwardly using

$$n^2(x) = [W_r(x) + jW_i(x)]^2 - \frac{j}{k_0}\frac{d}{dx}\left[W_r(x) + jW_i(x)\right]. \tag{2.50}$$

In order to fulfill the boundary conditions $W(-L) = W(L) = n_0$, $h(x)$ and $g(x)$ have to be constant at the beginning and at the end of the scattering region. While choosing $g(x)$ and $h(x)$, one has to consider that $n_r(x)$ has to be larger than 1, since for some combinations of $g(x)$ and $h(x)$ this is not the case. In Fig. 2.6 we can see a wave propagating through a system with a refractive index derived from given functions $g(x)$ and $h(x)$. The numerically calculated scattering wave function indeed shows the predicted phase profile $h(x)$ and intensity profile $g^2(x)$.

To sum up, one can design a refractive index $n(x)$ such that the wave inside has a well-defined amplitude profile $g(x)$ and phase profile $h(x)$ for one specific wavenumber k_0. One can use this procedure to create a scattering state that has a well-defined intensity profile, since the intensity is just given by $|\psi(x)|^2 = g^2(x)$.

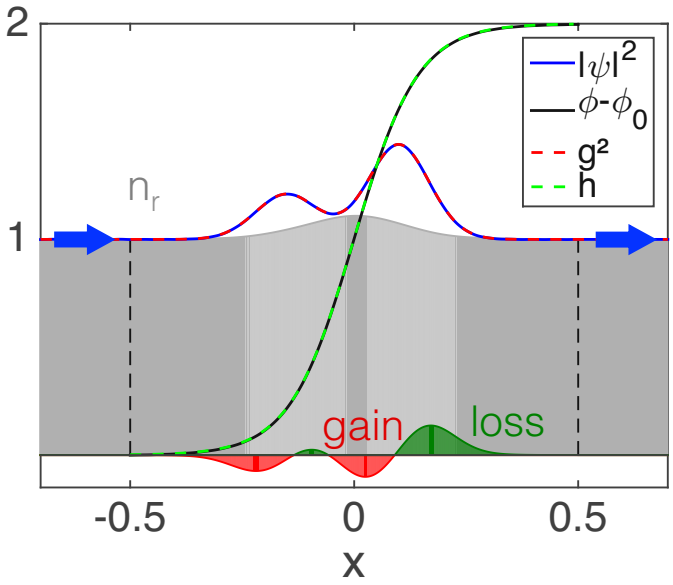

Figure 2.6: Using the idea of complex generating functions $W(x)$, one can calculate a refractive index, such that the wave function inside the medium has a predefined amplitude and phase profile, $\psi(x) = g(x)e^{jh(x)}e^{jk_0n_0x}$. The given function $g(x)$ and $f(x)$ are used to calculate the required refractive index (2.50). Here, $g(x)$ is the sum of two Gaussian functions with different amplitudes and positions, and $h(x)$ has the form of a hyperbolic tangent. The numerically calculated intensity, $|\psi(x)|^2$ (blue line), and additional phase, $\phi(x) - \phi_0(x)$ (black), agree with the analytic functions $h(x)$ (green) and $|g(x)|^2$ (red). $\phi_0(x)$ is the phase that the wave would accumulate in a uniform material with refractive index n_0, i.e., $\phi_0(x) = k_0n_0x$. Gain and loss are multiplied by a factor of 5 for a better visibility. The incident wave has a wavenumber of $k_0 = 2\pi/0.1$.

Constant-intensity waves can then be seen as the special case where $g(x) = 1$. It is important to mention that these scattering states are reflectionless, so that we found a whole new class of reflectionless refractive indices. After giving a detailed and extensive theoretical description of constant-intensity waves in the last sections, we present possible experimental realizations considering experimental limitations in the last part of this chapter.

2.8 Possible Experimental Realizations

Designing a material with a varying Hermitian refractive index is already a challenging task but in combination with a varying gain and loss distribution, the challenge becomes very demanding. Especially with the realization of amplifying regions, we are facing a great experimental difficulty that can be alleviated when using some tricks to create an effective constant-intensity refractive index by using only loss.

In order to calculate a refractive index distribution featuring only loss, we make use of the concept of complex generating functions $W(x) = W_r(x) + jW_i(x)$, as introduced in the previous section. Assuming that $W_i(x) = \text{const} = \kappa$, we get $\psi(x) = e^{jk_0 \int W_r(x')dx'} e^{-k_0 \kappa x}$, i.e., an exponentially decaying wave function where the factor $k_0\kappa$ determines the strength of the decay. Calculating the corresponding refractive index

$$n^2(x) = [W_r(x) + j\kappa]^2 - \frac{j}{k_0}\frac{d}{dx}[W_r(x) + j\kappa], \tag{2.51}$$

one can now choose κ and $W_r(x)$, such that the imaginary part of $n(x)$ is always larger than 0, i.e., always lossy. In Fig. 2.7(a) we plot a (normal) constant-intensity refractive index with the corresponding constant-intensity wave, whereas in Fig. 2.7(b) we show an exponentially decaying wave function in a completely lossy medium with refractive index (2.51). The small reflections at the beginning of the potential region come from the fact that the boundary conditions $W(-L) = W(L) = 1$ are not fulfilled, since the imaginary part of $W(x)$ is not zero at the beginning and at the end of the potential region. Since the imaginary part $n_i(x)$ is small compared to the real part $n_r(x)$, the error is negligible and only leads to small reflections. This idea of shifting the imaginary part of the refractive index such that everything becomes lossy is a possible candidate for an experimental implementation and still proves the concept of constant-intensity waves.

The second idea in the direction of a realizable system involves only loss as well, but contrary to the first concept, shows a true constant-intensity wave. We make use of the fact that a constant-intensity wave is a wave propagating into one direction without having back reflections at any part of the medium. Thus, we can truncate the system at any point and still get a constant-intensity wave, provided one continues the system with a constant generating function that has the same value as

at the point of truncation. Starting from the single-hump constant-intensity refractive index in Fig. 2.7(c), one can set the generating function $W(x)$ constant from the beginning of the potential region to its center. A constant generating function results in a vanishing imaginary part, so that we can eliminate the gain part, as can be seen in Fig. 2.7(d). The boundary conditions $W(-L) = W(L) = 1$ have to be generalized to $W(-L) = n_0(-L)$ and $W(L) = n_0(L)$, where $n_0(-L)$ and $n_0(L)$ is the (real) refractive index of the uniform material in front of and behind the potential region, respectively. Using this simple trick allows us to realize a CI wave in a loss-only material.

After presenting two methods for the implementation of constant-intensity waves with only lossy regions, we now also discuss the implementation of gain regions. Amplifying materials are used in lasers, where the gain medium is pumped to produce a population inversion. In order to achieve position-dependent amplification, which is necessary for constant-intensity refractive indices, one can optically pump a gain medium non-uniformly with the help of spatial light modulators (SLM). In combination with position depended loss regions, an implementation of full CI refractive indices is thus possible in principle.

To summarize, in this last section we show that an experimental realization of constant-intensity waves is within reach of current technology. The relation to unidirectional invisibility, supersymmetry and $\mathcal{PT}$-symmetry are just some of many striking features of these new types of waves suggesting that there is still a lot to discover. Having shown that a Hermitian refractive index in combination with a tailored gain/loss distribution can lead to this striking phenomenon, the second part of this thesis follows quite the opposite approach. Instead of controlling the medium itself, e.g., through a spatially modulated pumping, we now focus instead on controlling the incident wave front to achieve a desired intensity distribution of the wave inside the scattering region. This can be done with the knowledge of asymptotic quantities alone, e.g., the scattering matrix S which is already accessible in experiments.

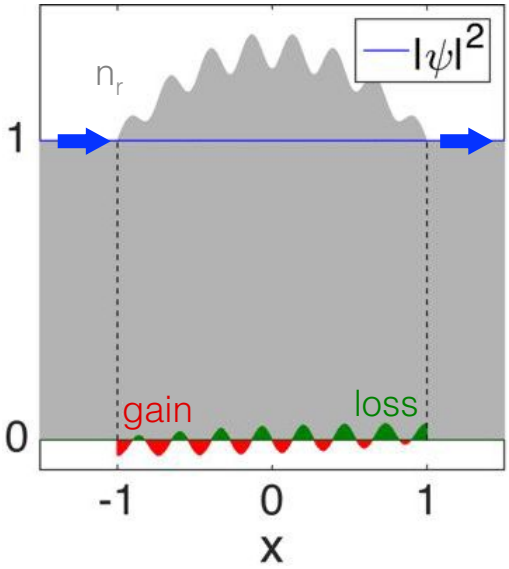

(a) Constant-intensity refractive index derived from a generating function with the shape of a parabolic function modulated with a cosine. For better visibility, gain and loss are multiplied by a factor of 10.

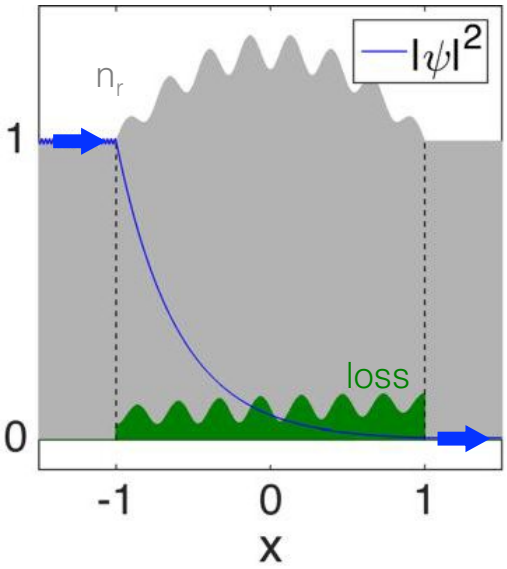

(b) Modified constant-intensity refractive index according to Eq. (2.51) with $W_i = \kappa = 0.01$. Due to the complex generating function $W(x) = W_r(x) + jW_i(x)$, we get uniform absorption, i.e., $\psi(x) = e^{jk_0 \int W_r(x')dx'} e^{-k_0 \kappa x}$. The reflections at the interfaces between potential region and free space come from the fact that the boundary conditions are not fulfilled, since the imaginary part of W is not zero at $-L$ and L. Also here, loss is multiplied by a factor of 10.

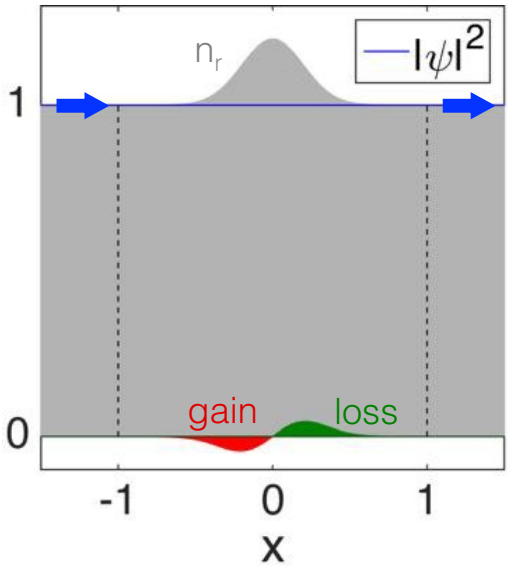

(c) Constant-intensity refractive index derived from a generating function with the shape of a Gaussian. For better visibility, gain and loss are multiplied by a factor of 10.

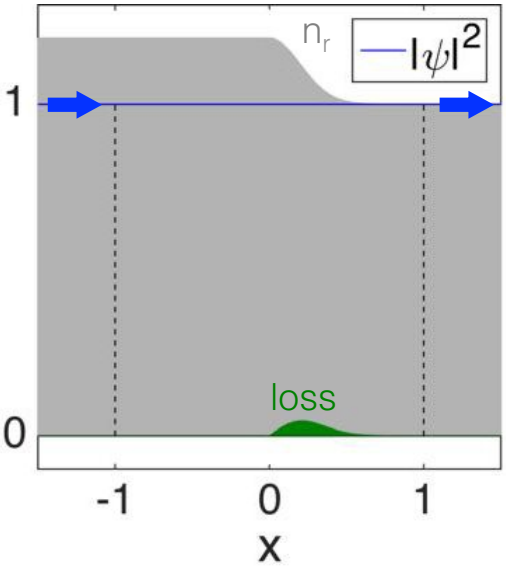

(d) Since constant-intensity systems can be truncated at any point and still lead to a wave with constant-intensity, we can set the first half of the generating function $W(x)$ to a constant value, and thus eliminating the gain part. Also here, loss was multiplied by a factor of 10.

Figure 2.7

Chapter 3

Wave Front Shaping

In the same way as the initial conditions of a classical particle, i.e., the particle's position and momentum at time t_0, determine its trajectory for all times $t > t_0$, providing the initial shape of an incident wave front can be used to describe the wave's future behavior due to the deterministic nature of wave scattering. However, interference effects may generally lead to highly complex intensity patterns. The concept of modulating the incident wave front in order to generate a specific behavior is better known as "wave front shaping" and has become a broad and fruitful field in modern wave physics during the last few years. The experimental accessibility of the scattering matrix in optics due to the availability of spatial light modulators (SLM), which are tunable pixel arrays that allow to create arbitrarily complex light fields, is one of the principal reasons for this progress. Wave front shaping can be used, e.g., to focus light, temporally as well as spatially, and to image and transmit light through media (see Ref. [39] and Refs. therein). In this chapter, we study and physically motivate all steps that are necessary in order to end up with the information on how to shape the incident wave front to create a specific desired scattering state. We discuss three concrete systems in which wave front shaping can be applied and perform all the preliminary calculations that are necessary to show that our procedure can be implemented experimentally. To be more specific, we show how to create scattering states that show beam-like behavior, focus on or avoid a chosen scatterer inside a scattering medium and turn a dissipative system into a coherent perfect absorber. In collaboration with Ulrich Kuhl's group at the University of Nice, we have been working on an experimental realization of these three systems in microwave cavities and are already able to show some first promising experimental results of two of those systems. Encouraged by these results, possible further applications are discussed at the end of each section. We start with a short introduction to the scattering formalism including the scattering matrix, which is used as a tool to construct these new scattering states.

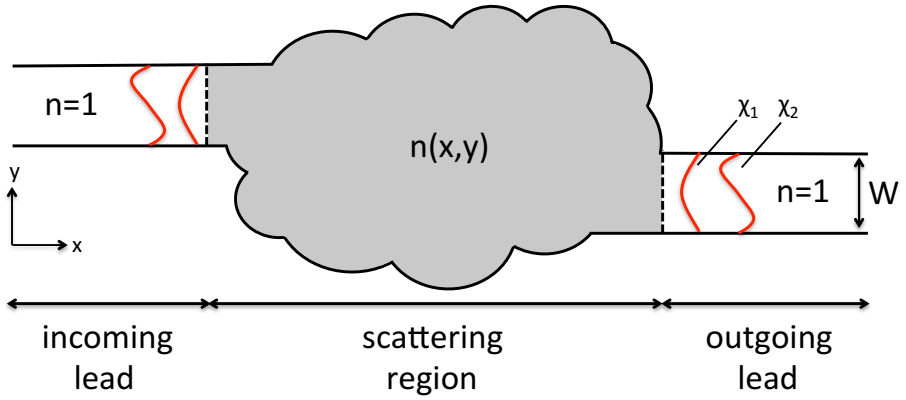

Figure 3.1: Our scattering systems can be decomposed into a scattering region (gray) and asymptotic regions (incoming and outgoing leads). Both leads are assumed to be clean, i.e., have a refractive index of $n = 1$ and are semi infinite. Incoming and outgoing lead have the same width W and the first two lead modes χ_1 and χ_2 are depicted in red. We use hard-wall boundary conditions at the borders of all our geometries.

3.1 Scattering Formalism

Generic scattering systems can be divided into the scattering region, where the actual scattering process takes place, and the asymptotic regions, where the wave can be decomposed into well-defined scattering channels. The systems we are interested in can be decomposed into an incoming lead, the scattering region and an outgoing lead. Incoming as well as outgoing lead are the asymptotic regions and are usually clean, i.e., they feature a refractive index of $n = 1$. The scattering region itself can be arbitrarily complex and can lead to strong scattering of the incoming wave. For the scattering geometries used later on, incoming and outgoing lead have the same width W and hard-wall boundary conditions are used at the borders of the geometry as we can see in Fig. 3.1.

Since we investigate stationary scattering systems, the starting point for our calculation is the two-dimensional (2D), time-independent Helmholtz equation

$$[\triangle + n^2(\vec{r})k^2]\psi(\vec{r}) = 0, \tag{3.1}$$

where $k = \frac{2\pi}{\lambda} = \sqrt{k_x^2 + k_y^2}$ is the vacuum wavenumber, λ the wavelength, $\triangle = \frac{d^2}{dx^2} + \frac{d^2}{dy^2}$ the Laplacian in $2D$, $n(\vec{r})$ the index of refraction, $\psi(\vec{r})$ the linearly polarized perpendicular component of the electric field, and $\vec{r} = (x,\ y)^T$ the position vector. Since incoming and outgoing lead are both clean, the right-propagating solutions of the Helmholtz equation take the following form,

$$\psi_n(x, y) = \frac{1}{\sqrt{k_{x,n}}}\chi_n(y)e^{jk_{x,n}x}, \tag{3.2}$$

where

$$\chi_n(y) = \sqrt{\frac{2}{W}} \sin(k_{y,n} y), \tag{3.3}$$

is the transverse part of the electric field and the corresponding left-propagating solutions are given by $\psi_n^*(x, y)$. The prefactor in Eq. (3.2), $1/\sqrt{k_{x,n}}$, ensures that every mode carries the same flux. The solutions (3.2) are called modes and are characterized by an integer n, the wavenumber in transverse direction

$$k_{y,n} = \frac{n\pi}{W}, \tag{3.4}$$

and the wavenumber in longitudinal direction

$$k_{x,n} = \sqrt{k^2 - k_{y,n}^2}. \tag{3.5}$$

For $k \geq k_{y,n}, k_{x,n}$ is real and the mode can propagate in x-direction, whereas if $k < k_{y,n}, k_{x,n} = j\kappa_{x,n}$ is purely imaginary and the mode decays exponentially, i.e., is an evanescent mode. Modes with $k_{x,n} \in \mathbb{R}$ can carry electromagnetic flux and are referred to as open modes, whereas evanescent modes are not flux-carrying. The number of open modes in either lead $N = N_{in} = N_{out}$ is determined by

$$N = \lfloor \frac{Wk}{\pi} \rfloor = \lfloor \frac{2\nu W}{c} \rfloor, \tag{3.6}$$

where ν is the frequency, c the speed of light and $\lfloor ... \rfloor$ the floor function. The transverse profiles (3.3) of the lead modes form a complete and orthonormal basis so that they can be used to decompose an arbitrary incoming wave into these basis functions. The incoming wave can then be written as a coefficient vector $\vec{\phi} = (\vec{\phi}_l,\ \vec{\phi}_r)^T$, where $\vec{\phi}_l$ contains the respective coefficients corresponding to the incoming wave coming from the left-hand side and, analogous, $\vec{\phi}_r$ the incoming wave coming from the right-hand side. The corresponding outgoing wave can be written as $\vec{\mu} = (\vec{\mu}_l,\ \vec{\mu}_r)^T$ and is connected to the incoming wave $\vec{\phi}$ through the scattering matrix, $\vec{\mu} = S\vec{\phi}$. Since for most of the presented systems we consider injection only from the left-hand lead, we refer to it as the incoming lead, while the right-hand lead is labeled as the outgoing one. Whereas the right-propagating parts $\vec{\phi}_l$ and $\vec{\mu}_r$ refer to the right-propagating lead modes ψ_n, the left-propagating parts $\vec{\phi}_r$ and $\vec{\mu}_l$ refer to the left-propagating lead modes, ψ_n^*. The scattering matrix S for our two-port system has the block structure

$$S = \begin{pmatrix} r_l & t_r \\ t_l & r_r \end{pmatrix}, \tag{3.7}$$

where r_l, t_l are the reflection and transmission matrices containing the scattering amplitudes for injection from the left side and r_r, t_r consist of the corresponding

amplitudes for injection from the right side. If we mention the transmission matrix t and the reflection matrix r, we usually refer to t_l and r_l, respectively, since for most of the systems we only consider injection from the left-hand lead. The matrix element t_{mn}, for example, is the complex amplitude for the transmission from the n-th incoming mode into the m-th outgoing mode. In Hermitian systems, i.e., systems without gain and loss, the scattering matrix S is unitary, $S^{-1} = S^\dagger$, and is therefore flux-conserving. If time reversal symmetry is not broken, which is the case in all our investigated systems, one can easily show that the following symmetry relations are valid: $r_l = r_l^T$, $r_r = r_r^T$, $t_l = t_r^T$.

In the following sections, we use the information stored in the scattering matrix S to shape the wave front of the incoming wave such that the wave shows a desired behavior *inside* the scattering region although the scattering matrix consists exclusively of information available *outside* of the scattering region, i.e., in the asymptotic regions. Our computer code which simulates the scattering systems automatically calculates the scattering matrix S for a given incident wavelength by using the modular recursive Green's function method introduced in Ref. [40]. In the next section we recall an operator, the Wigner-Smith time-delay operator, of which the eigenvectors contain the information on how to shape the incident wave front to get beam-like scattering states. After that, we introduce a new operator class that combines an elegant theoretical concept with experimental practicability.

3.2 Wigner-Smith Time-Delay Operator Q_ω

As numerically shown by Rotter et al. [23], wave front shaping can be used to create so-called particle-like states which are scattering states that feature beam-like behavior. If a wave enters a cavity, it may generally get reflected multiple times so that the wave function will be distributed throughout the cavity. The wave function of particle-like states, however, stays highly collimated along its path, or to be more precise, the wave function occupies a bundle of classical trajectories that have similar lengths. These particle-like states can be found among the eigenvectors of the Wigner-Smith time-delay operator,

$$Q_\omega = -jS^\dagger \frac{dS}{d\omega} = \begin{pmatrix} Q_{11} & Q_{12} \\ Q_{21} & Q_{22} \end{pmatrix}, \tag{3.8}$$

that was proposed by Smith [41] after the seminal work of Eisenbud, Bohm [42] and Wigner [43], where S is the scattering matrix and ω the frequency. In practice, the derivative in Eq. (3.8) is usually approximated by a finite difference quotient $\frac{dS}{d\omega}|_{\omega=\omega_0} \approx \frac{S(\omega_0+\Delta\omega)-S(\omega_0)}{\Delta\omega}$, where $\Delta\omega$ is sufficiently small. Calculating the expecta-

tion value of Q_ω for an input vector $\vec{\phi}$ yields [44],

$$\tau_Q = \sum_{i=1}^{N_{in}+N_{out}} |(S\vec{\phi})_i|^2 \frac{d\varphi_i}{d\omega}, \tag{3.9}$$

where $N_{in} + N_{out}$ is the total number of flux-carrying channels (for systems with both sides of injection) and φ_i the phase of $(S\vec{\phi})_i = |(S\vec{\phi})_i|e^{j\varphi_i}$. The operator (3.8) is based on the idea that the frequency derivative of the scattering phase φ_i can be interpreted as the time it takes the wave to traverse the scattering region. The expectation value (3.9) can thus be seen as a weighted sum of the delay times of every scattering channel, where the weighting coefficients are the corresponding absolute values of the scattering amplitudes. Eigenvectors of this Wigner-Smith time-delay operator thus have a well-defined delay time, just like a particle traveling through a system. Since Q_ω is a Hermitian operator, its eigenvalues are real-valued and thus can be interpreted as the correct physical delay times. Particle-like states are those eigenvectors of Q_ω that are simultaneously eigenvectors of the sub block $Q_{11} = -j(r^\dagger \frac{dr}{d\omega} + t^\dagger \frac{dt}{d\omega})$ and additionally lie in the nullspace of Q_{21} [23].

With respect to an experimental realization of such particle-like states, the Wigner-Smith time-delay operator suffers from a major drawback. The construction of Q_{11} involves the transmission matrix t as well as the reflection matrix r, where the latter one is often hard to measure in experiments, therefore, we propose an alternative operator involving only the transmission matrix t,

$$q_\omega = -jt^{-1}\frac{dt}{d\omega}. \tag{3.10}$$

Contrary to the Wigner-Smith time-delay operator Q_ω, the operator q_ω is generally not Hermitian and thus has complex eigenvalues. In the event that the transmission matrix is unitary, $t^{-1} = t^\dagger$, however, q_ω coincides with the Hermitian sub-block Q_{11} of the Wigner-Smith matrix, $Q_{11} = q_\omega$. In the following, we motivate the specific shape of (3.10) and generalize this operator to a new operator class that yields scattering states that are invariant to first order against the change of an arbitrary parameter [45], and show that q_ω is just one example of this class.

3.3 Phase Derivative Operator q_a

In the fiber community, eigenstates of the operator q_ω are known as so-called principal modes and are invariant to first order under a variation of the frequency [46, 47]. In the following, we show an alternative derivation of this operator (but still follows the spirit of the derivation in Ref. [47]) and generalize this concept to systems with an arbitrary parameter dependence, which in the case of q_ω is the frequency ω.

Suppose we have an incoming wave injected from the left-hand lead characterized by a coefficient vector $\vec{\phi}_l$, we can calculate the output vector to the right (transmitted part), $\vec{\mu}_r = t\vec{\phi}_l$. Assuming that the transmission matrix t depends on an arbitrary continuous parameter a, e.g., the incoming frequency ω, the position of an arbitrary scatterer $\vec{r}$ that is located inside the scattering region or the strength of an external magnetic field $|\vec{B}|$ (in the context of charged matter waves), one can approximate the output vector $\vec{\mu}_r$ in the vicinity of a specific value of $a = a_0$ by a Taylor series,

$$\vec{\mu}_r(a_0 + \Delta a) = \vec{\mu}_r(a_0) + \Delta a \left.\frac{d\vec{\mu}_r}{da}\right|_{a_0} + \dots \tag{3.11}$$

$$= t(a_0)\vec{\phi}_l + \Delta a \left.\frac{dt(a)}{da}\right|_{a_0} \vec{\phi}_l + \dots, \tag{3.12}$$

where Δa is a small change of the parameter a and we assumed that the input vector $\vec{\phi}_l$ does not depend on a. We demand that the first oder term is parallel to the zeroth order term, i.e., they should only differ by a multiplicative (complex) constant z,

$$t(a_0)\vec{\phi}_l = z\Delta a \left.\frac{dt(a)}{da}\right|_{a_0} \vec{\phi}_l. \tag{3.13}$$

Multiplying both sides of Eq. (3.13) with $(jt)^{-1}$, one can rewrite it as an eigenvalue equation,

$$\frac{1}{jz\Delta a}\vec{\phi}_l = -jt^{-1}(a_0) \left.\frac{dt(a)}{da}\right|_{a_0} \vec{\phi}_l = \tau_a\vec{\phi}_l = q_a\vec{\phi}_l, \tag{3.14}$$

where $\vec{\phi}_l$ can now be seen as the eigenvector of the operator

$$q_a := -jt^{-1}\frac{dt}{da} \tag{3.15}$$

with the eigenvalue $\tau_a := (jz\Delta a)^{-1}$.

Just as the eigenvalues of the Wigner-Smith operator are proportional to the frequency derivative of the scattering phase, we now try to find a mathematical expression for the eigenvalues of q_a, τ_a, in order to ascribe to them a physical interpretation. Going back to Eq. (3.13) with $z = (j\tau_a\Delta a)^{-1}$,

$$\tau_a t\vec{\phi}_l = -j\frac{dt(a)}{da}\vec{\phi}_l, \tag{3.16}$$

$$\tau_a\vec{\mu}_r = -j\frac{d\vec{\mu}_r}{da}, \tag{3.17}$$

we can decompose the output state according to

$$\vec{\mu}_r = \hat{\mu}_r|\vec{\mu}_r|e^{j\phi_\mu}, \tag{3.18}$$

where $\hat{\mu}_r$ is the unit vector pointing in the direction of $\vec{\mu}_r$, φ_μ is a global phase and $|\vec{\mu}_r|$ the global amplitude of $\vec{\mu}_r$. We see in the end that the actual value of the global phase does not matter, since it can be chosen arbitrarily, however, its derivative will be of interest. Inserting Eq. (3.18) into (3.17), yields

$$\begin{aligned}\tau_a \hat{\mu}_r |\vec{\mu}_r| e^{j\varphi_\mu} &= -j\left(|\vec{\mu}_r| e^{j\varphi_\mu}\frac{d\hat{\mu}_r}{da} + \hat{\mu}_r e^{j\varphi_\mu}\frac{d|\vec{\mu}_r|}{da} + j\hat{\mu}_r|\vec{\mu}_r|e^{j\varphi_\mu}\frac{d\varphi_\mu}{da}\right),\\ \tau_a &= -j\frac{1}{|\vec{\mu}_r|}\left(\frac{d|\vec{\mu}_r|}{da} + j|\vec{\mu}_r|\frac{d\varphi_\mu}{da}\right) = -j\frac{1}{|\vec{\mu}_r|}\frac{d|\vec{\mu}_r|}{da} + \frac{d\varphi_\mu}{da}\\ &= -j\frac{d\ln(|\vec{\mu}_r|)}{da} + \frac{d\varphi_\mu}{da}, \end{aligned} \tag{3.19}$$

where we used $\frac{d\hat{\mu}_r}{da} = 0$, since we started our derivation calling for output states that are independent of a (up to a global phase and amplitude). The first term of the eigenvalue τ_a on the right-hand side of Eq. (3.19) describes the change of the transmission of the eigenstate as a function of a, whereas the second term is the derivative of the global scattering phase with respect to a.

As mentioned above in the derivation of Eqs. (3.19) and (3.15), we assume the scattering matrix t to be invertible. If t is not quadratic or singular due to channels with transmission close to zero, however, an ordinary inversion cannot be done. For that reason, an effective inversion, introduced by Philipp Ambichl and shown in our work [48], that involves a projection of the transmission matrix onto transmitting channels is presented in the following. We start with a singular value decomposition of the transmission matrix,

$$t = U\Sigma V^\dagger, \tag{3.20}$$

where U consists of the eigenvectors of $tt^\dagger$ stored in its columns and V consists of the eigenvectors of $t^\dagger t$, respectively. For a $m \times n$-dimensional transmission matrix, the matrices U and V are quadratic $m\times m$ and $n\times n$ matrices, respectively, whereas Σ is an $m \times n$-dimensional rectangular matrix which contains the singular values σ_i, i.e., the square roots of the (common) eigenvalues of both $t^\dagger t$ and $tt^\dagger$, on its diagonal. The relative phases of U and V can be chosen such that Σ contains only real quantities. If t is singular or non-quadratic, at least one singular value is zero. In order to get rid of those states that belong to $\sigma = 0$, we keep only those n_ϵ columns of U and V that belong to singular values larger than a specific value ϵ and group them to new matrices u and v which then have the dimensions $m \times n_\epsilon$ and $n \times n_\epsilon$, respectively. Since numerically the singular values of low transmitting channels will never be exactly zero, ϵ has to be chosen finite, but small. In a next step we project the full transmission matrix t onto the kept transmitting channels according to

$$\tilde{t} = u^\dagger t v, \tag{3.21}$$

so that we end up with a quadratic $n_\epsilon \times n_\epsilon$-dimensional matrix. Inverting $\tilde{t}$, which is now possible, and projecting back onto the original vector space gives the effective

inversion which we are looking for,

$$t_\epsilon^{-1} := v(u^\dagger t v)^{-1} u^\dagger. \tag{3.22}$$

If there are no singular values smaller than a chosen value of ϵ, t_ϵ^{-1} coincides with the ordinary inversion t^{-1}. In a next step, using the projection operators $uu^\dagger$ and $vv^\dagger$, we can project the derivative in (3.15) of the transmission matrix onto the flux-carrying channels

$$\frac{dt_\epsilon}{da} = uu^\dagger \frac{dt}{da} vv^\dagger, \tag{3.23}$$

so that we end up with the final expression for the operator q_a that involves only states featuring a transmission larger than ϵ,

$$q_a = -jv(u^\dagger t v)^{-1} u^\dagger u u^\dagger \frac{dt}{da} vv^\dagger = -jv(u^\dagger t v)^{-1} u^\dagger \frac{dt}{da} vv^\dagger. \tag{3.24}$$

In Eq. (3.24) we made use of the fact, that $u^\dagger u = \mathbb{1}_{n_\epsilon \times n_\epsilon}$, but please note that generally $uu^\dagger \neq \mathbb{1}_{m\times m}$.

With expression (3.24) we develop a method to calculate eigenstates of the operator q_a in Eq. (3.15) for systems with a singular or non-quadratic transmission matrix. Since the parameter a can be chosen arbitrarily, we introduce a whole new operator class that leads to scattering states that are invariant against changes of a to first order. The time-delay operator q_ω, which we mention in the previous section, is just one example of this class for the case that the continuous parameter is the frequency, $a = \omega$. The eigenvalues of q_ω are given by Eq. (3.19) and thus include the frequency derivative of the global scattering phase which resemble the expectation value of the Wigner-Smith time-delay operator in (3.9) containing the frequency derivatives of the individual scattering channels. Instead of using the Wigner-Smith time-delay operator, we show in the next section that q_ω can be used to find particle-like states as well but brings a major benefit in terms of an experimental realizability.

3.4 Particle-Like States as Eigenstates of q_ω

Particle-like scattering states can be found among the eigenstates of the sub-block of the Wigner-Smith time-delay operator (3.8), Q_{11}, however, the knowledge of the transmission matrix t and the reflection matrix r is necessary. The operator introduced in the previous section, q_ω, suggests that particle-like states can be constructed solely from the knowledge of the transmission matrix t, since its eigenvalues are proportional to the frequency derivative of the scattering phase (i.e., the delay time), similar to the concepts involved in the construction of the Wigner-Smith time-delay operator. In what follows, we study the new operator q_ω right for a

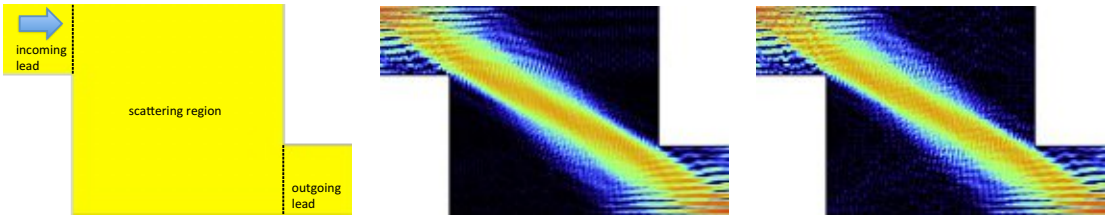

(a) (b) (c)

Figure 3.2: (a) Scattering geometry in which particle-like states should be observed. The left upper lead is the incoming lead whereas the right lower lead the outgoing one. The region between the dashed lines represents the scattering region. (b) Eigenstate of the Wigner-Smith time-delay operator Q_ω and (c) the corresponding eigenstate of the operator q_ω, where all singular values larger than $\epsilon = 0.1$ were kept for the projection in (3.24). In (b), both, the reflection matrix r and the transmission matrix t were used, whereas (c) involves only the transmission matrix t. Both operators lead to the desired particle-like scattering state, however, the operator q_ω requires less information. The incoming wavelength was chosen such that 16 modes are open in the leads.

specific system shown in Fig. 3.2(a); Fig. 3.2(b) shows a particle-like eigenstate of the Wigner-Smith time-delay operator, whereas Fig. 3.2(c) shows the corresponding eigenstate of q_ω. We can see that the operator q_ω, which only involves the transmission matrix t, indeed leads to almost the same result with respect to this particle-like state as the Wigner-Smith time-delay operator does, although it requires less information. This encouraging observation brings us one step closer to an experimental realization of such beam-like scattering states.

Measuring the transmission matrix t and shaping the wave front of the incoming wave with multiple separate antennas is experimentally already possible in the microwave regime. In a collaboration with the group of Ulrich Kuhl from the University of Nice, we designed a concrete experimental set-up in which particle-like states can be realized. All effects of imperfections, that an experiment typically comes along with, are investigated and quantified in the following subsection.

3.4.1 Particle-Like States in a Specific System

The major achievement presented in this subsection is to design a scattering geometry that takes into consideration all experimental limitations, such as the number of antennas, the size of the experimentation table or the maximum frequency while still allowing for particle-like states. The first obstacle in realizing particle-like states has already been overcome by finding an operator that can be constructed

with the transmission matrix t exclusively, since reflections are hard to measure in many experimental setups, including our microwave setups at hand. The main limitation in our experiment, however, is the size of the experimentation table and the number of available antennas. The more modes or antennas can be controlled independently in phase and amplitude, the better and clearer the particle-like states will be. The number of available antennas, which is restricted to 16, is therefore a critical factor for the design of the experiment.

Please note that the concept of finding particle-like states is basis independent, i.e., it does not matter if the transmission matrix t is measured and transformed to the basis of waveguide modes or if the measured antenna-antenna signals are used directly, which facilitates the experiment.

To state the experimental limitations more precisely, the region of which the wave function can be measured is limited to an area of 104×52 cm, as indicated in Fig. 3.3. To avoid an undesired influence of evanescent modes, the antenna array has to be placed with a distance of 1.5 times the lead width W away from the entry to the scattering region, and about the same distance away from the other end, where absorbers are placed to reduce reflections. The effective size of the whole system including both leads is therefore much larger than just the size of the scattering region alone. The minimum size of the lead width is restricted by two parameters: On the one hand, the mounting system of the antennas requires a minimum distance of 0.7 cm between each antenna, which leads to a minimum lead width of approximately 12 cm for a number of 16 antennas. On the other hand, the most efficient control of the wave is ensured if the number of antennas is equal to the number of flux-carrying modes, since for this case all degrees of freedom can be controlled. The number of open modes N is determined by the input frequency ν, according to Eq. (3.6). Since the maximum frequency in the experiment is $\nu_{max} = 18$ GHz, the minimum lead width has to be around 14 cm to ensure that 16 modes are open. A non-trivial geometry we found that even features chaotic classical dynamics and additionally considers all the limitations but still allows for particle-like states is shown in Fig. 3.3, where the left top lead is the incoming lead, and the right lower lead is the outgoing one, respectively. In Fig. 3.4(a) we can see a simulation where the first mode is injected into the system and strongly scattered, whereas in Fig. 3.4(b)-(d) we can see three eigenstates of q_ω which are clearly particle-like. The first state propagates directly from the incoming to the outgoing lead, whereas the second one bounces off the quarter circle and the third one bounces off the upper boundary. In the following subsection, we refer to the particle-like states in Fig. 3.4(b)-(d) as states number 1 to 3.

If we keep n_ϵ singular values in the calculation of q_ω in (3.24), we get n_ϵ transmitting q_ω-eigenstates. Since the choice of ϵ, which determines how many singular values are kept for the calculation, is arbitrary, we calculate all possible eigenstates of q_ω for all possible numbers of kept singular values which gives a total number of $16 + 15 + 14 + ... + 1 = 136$ eigenstates. Measuring the wave function of all

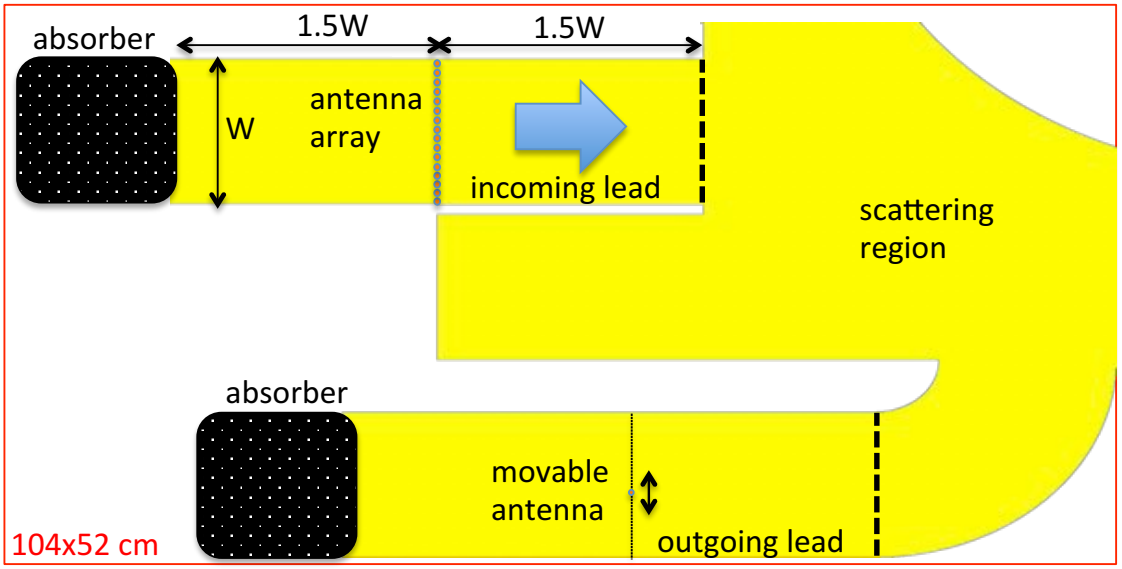

Figure 3.3: The scattering geometry that is used for the particle-like states experiment drawn on the experimentation table of size 104×52 cm (red rectangle). The lead width $W = 14$ cm and the frequency $\nu = 17.5$ GHz results in a total number of 16 open modes, which is equal to the number of antennas in the incoming channel. The distance of $1.5W$ between the antenna array and the main cavity prevents evanescent coupling to the system. Absorbing material at both ends of the system is used to suppress reflections. A movable antenna in the output lead is used in order to detect the output signal. The middle part of the scattering region between both leads can alternatively be used as an input lead. As can be seen, the whole scattering geometry is much larger than the actual scattering region within the black dashed lines.

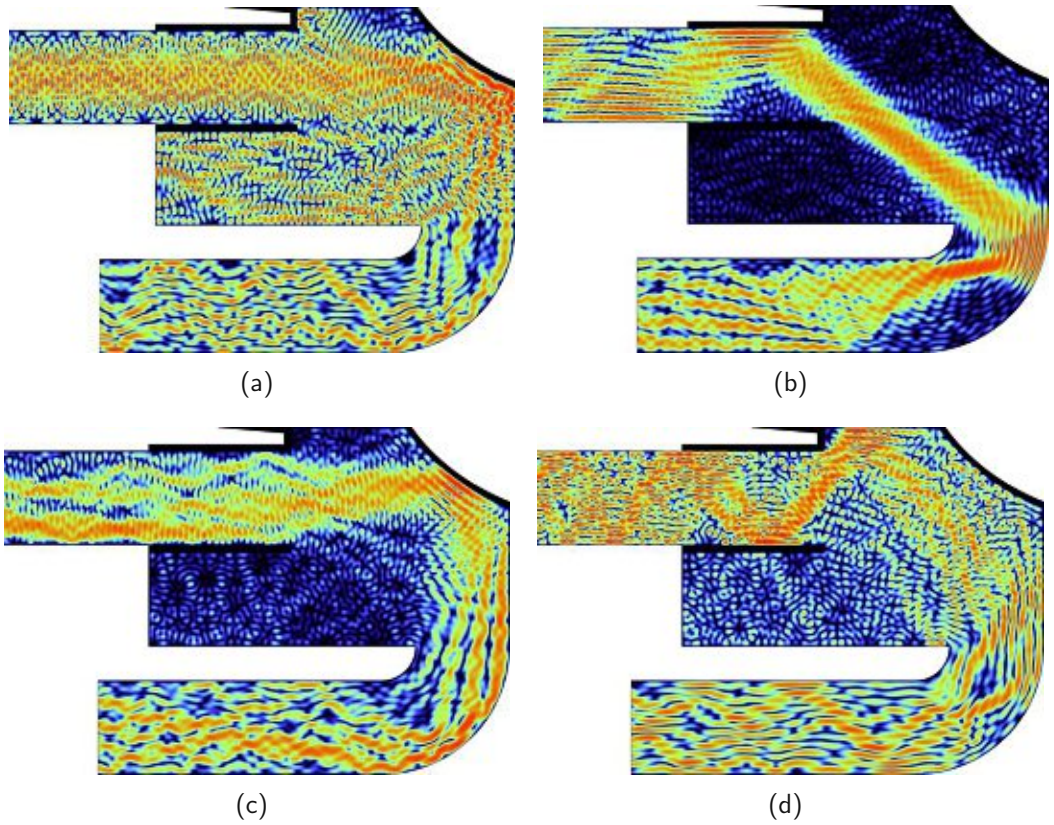

Figure 3.4: Numerical results: (a) Shows shows how the first transversal mode is injected and strongly scattered inside the system described in Fig. 3.3, whereas (b), (c) and (d) show three particle-like states which are eigenstates of the operator q_ω. For the calculation of q_ω, the smallest three singular values are neglected in (3.24).

those eigenstates to find particle-like states among them is practically impossible. Therefore, the question we are interested in answering is the following: is it possible to identify particle-like states among the eigenstates of q_ω, without knowing their respective wave functions inside the scattering region? Despite the wave function, a scattering state is characterized by its eigenvalue τ_ω and the transmittance. The real part of the eigenvalues τ_ω of q_ω is given by Eq. (3.19),

$$\mathrm{Re}(\tau_\omega) = \frac{d\varphi_\mu}{d\omega}, \tag{3.25}$$

which corresponds to the time it takes the wave to traverse the system, as discussed before. Since particle-like states are highly collimated, one can estimate their delay times by the length of the corresponding classical trajectories dividing it by the speed of light. q_ω-eigenstates with $\mathrm{Re}(\tau_\omega)$ close to this estimated value are likely to be particle-like. Furthermore, the imaginary part of τ_ω, which is given by Eq. (3.19),

$$\mathrm{Im}(\tau_\omega) = -\frac{d\ln(|\vec{\mu}_r|)}{d\omega}, \tag{3.26}$$

indicates how the transmitted intensity changes as a function of ω. Due to the classical character of particle-like states resulting in maximum transmission, the output intensity $|\vec{\mu}_r|^2$ is almost independent of the frequency ω, so that the derivative with respect to ω is small. All three indicators, i.e., a high transmission, a small imaginary part of τ_ω and a real part of τ_ω that can be estimated from the corresponding classical trajectory path, can be used to distinguish particle-like states from all the other eigenstates of q_ω without the time-consuming measurement of all wave functions.

We also numerically investigated the influence of absorption and noise with a noise amplitude of 10% of the signal, and found that those imperfections do not affect the stability of particle-like states significantly (not shown).

In this subsection we design a realizable set-up to observe particle-like states in the experiment under the given constraints of size, frequency, and number of controllable channels. All preliminary simulations prove that the set-up at hand is suitable for this kind of experiment. In the next subsection we present first results from the experiment conducted at the University of Nice.

3.4.2 Experimental Results

Ulrich Kuhl's group, who are real experts in microwave experiments, put much work and effort into realizing the set-up discussed in the previous subsection. The now presented results are preliminary and may differ from what will be published in a journal, however, we can already see a clear tendency towards particle-like behavior of some scattering states. To jump right to the results, Fig. 3.5(a) shows the direct particle-like state and Fig. 3.5(b) and Fig. 3.5(c) the states that bounce off the

boundary, respectively, which correspond to the states predicted in the simulations shown in Fig. 3.4(b), Fig. 3.4(c) and Fig. 3.4(d). The experimental results are in good agreement with our simulations thereby corroborating our theory.

After this encouraging proof of principle, we present possible applications of these beam-like scattering states in the next subsection.

3.4.3 Possible Applications of Particle-Like States

The highly focused wave function and the frequency stability of particle-like states indicate that a pulse propagating along one "trajectory" of a particle-like state can be possible, providing the opportunity to send information from one point to another one with minimal loss of the signal to the environment. A pulse $\psi(x, y, t)$ can be constructed from a coherent superposition of scattering wave functions with the same (particle-like) input vector $\vec{c} = (c_1, c_2, ...c_N)^T$ (N is the number of open modes) but at different frequencies by the Fourier transform,

$$\psi(x, y, t) = \frac{1}{\sqrt{2\pi}} \int_\omega A(\omega)\psi(x, y, \omega)e^{-j\omega(k)t}d\omega, \tag{3.27}$$

with $\omega(k) = kc$ and $\psi(x, y, \omega)$ being the scattering wave function at frequency ω. $A(\omega)$ is the weighting function defining the spectral shape of the pulse which we assume to have the form of a Gaussian,

$$A(\omega) = Ce^{-\frac{(\omega-\omega 0)^2}{2\sigma^2}}, \tag{3.28}$$

where ω_0 is the center frequency at which the input vector $\vec{c}$ is calculated, σ is the width of the Gaussian, and C a normalization factor. In practice, the integral in ω-space will turn into a sum,

$$\psi(x, y, t) = \tilde{C} \sum_{\omega=1}^{N_\omega} A_\omega \psi_\omega(x, y)e^{-j\omega(k)t}, \tag{3.29}$$

where N_ω is the number of superimposed wave functions at different frequencies ω weighted by the coefficients A_ω and $\tilde{C}$ is a normalization factor. In Fig. 3.6 we show pulses propagating along the trajectories of the already shown particle-like states 1 and 2 (see Fig. 3.4(b) and 3.4(c)) at three different time steps. The figures show that the pulses stay confined along the whole scattering region, proving the frequency stability of particle-like states.

In the course of secure information exchange, one wants to clarify if a possible eavesdropper has intruded into the system. Suppose information should be sent along the path of particle-like state number 1, but an eavesdropper is located somewhere along this path. Measuring the transmission matrix t of the new system, i.e., with perturbator, and calculating q_ω-eigenstates would not yield particle-like

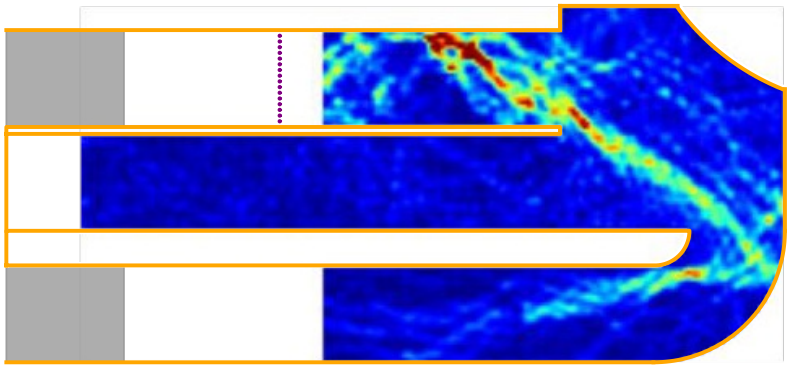

(a)

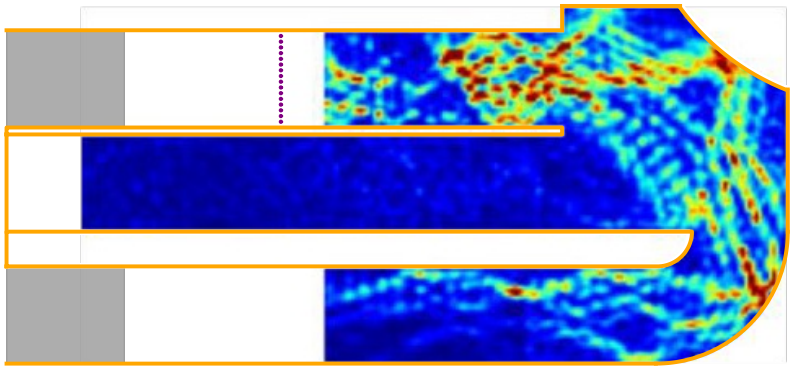

(b)

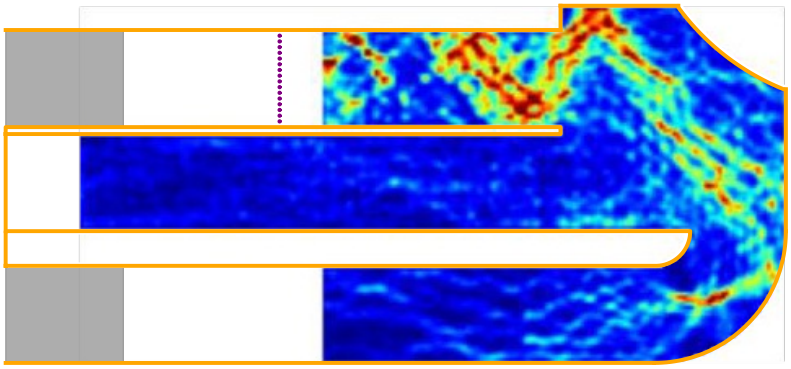

(c)

Figure 3.5: First experimental realization of the particle-like states predicted in Fig. 3.4(b)-(d). The set-up and the parameters are discussed in the previous subsection, whereas the distance between the antenna array (drawn in purple) and the actual scattering region as well as the rectangular region below the incoming lead have different dimensions. The absorbers are indicated by the grey shaded areas. The figures show the intensity of the wave function whereas an interpolation between the measurement points was done to smooth out the plot. Although these experimental results are only preliminary, they show already the predicted beam-like behavior. In (a), the five highest singular values are kept for the projection in Eq. (3.24), whereas in (b) and (c) we keep the seven highest singular values.

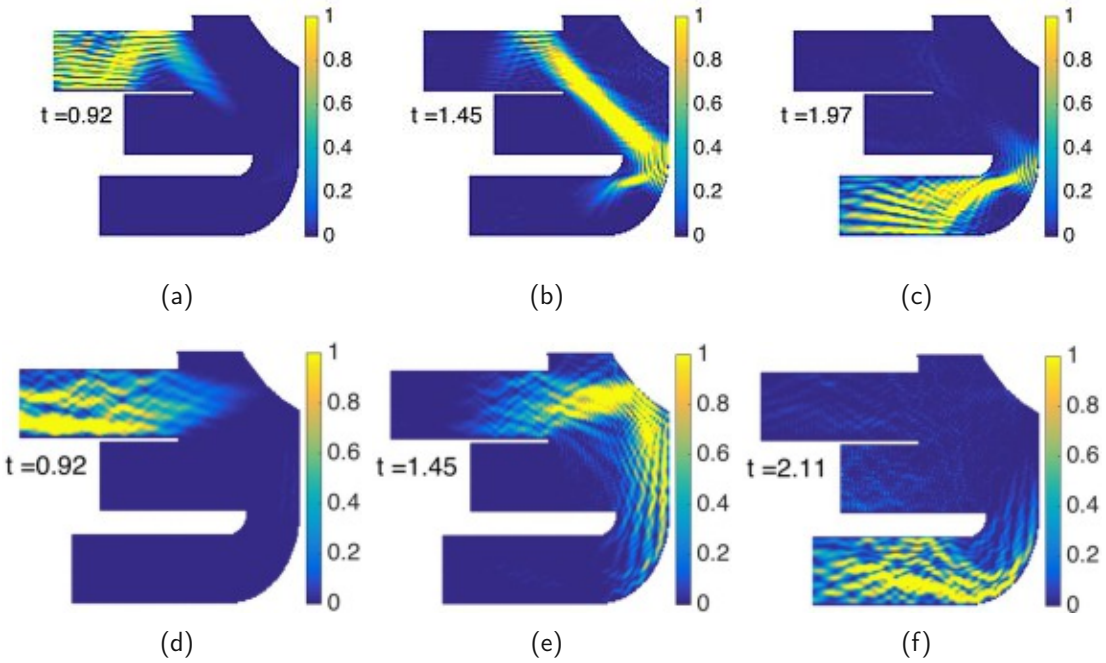

Figure 3.6: (a)-(c), (d)-(f) Two pulses propagating on the particle-like states shown in Fig. 3.4(b) and Fig. 3.4(c), respectively. Numerically, we calculate the input vector for the particle-like states on a center-frequency $\omega_0 = \frac{16.5\pi c}{W}$, where c is the speed of light and W the lead width, and inject the same input state at 20 frequency points in the interval $\omega \in [\frac{16.2\pi c}{W}, \frac{16.8\pi c}{W}]$. Then we superimpose the wave functions coherently according to Eq. (3.29). Due to reasons of practicability, we set the speed of light $c \equiv 1$ here.

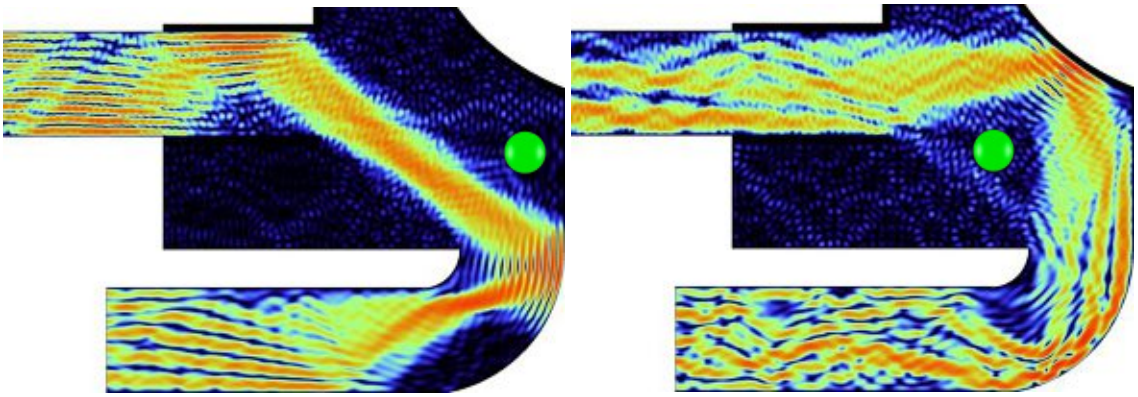

(a) (b)

Figure 3.7: (a) If an eavesdropper (green) is introduced into the system somewhere along the path of particle-like state number 2, the operator q_ω would not yield this particle-like state anymore, however, particle-like state number 1 can be found since this state is not affected by the obstacle. (b) Particle-like state number 2 which can be used for information exchange, if the eavesdropper blocks the path of particle-like state number 1.

state number 1 anymore. However, information could be sent along path number 2, which avoids the eavesdropper. In combination with a continuous measurement of the transmission matrix t, an eavesdrop-secure communication can be guaranteed by sending information along a particle-like state that passes by the eavesdropper, as can be seen in Fig. 3.7. One big advantage of this method is that the position of the eavesdropper does not have to be known by the transmitter, since particle-like states that are affected by the current position of the eavesdropper would not be "found" by the algorithm. However, particle-like states that are not affected by the eavesdropper can be identified by their eigenvalues as discussed in the previous subsection and will be used to send information.

In this subsection we discuss possible applications of particle-like states and numerically prove their applicability in the set-up which we design in the previous subsection. Particle-like states are found numerically among the eigenstates of the operator q_ω, which have a well-defined delay time. Please note that the phase derivative operator q_a in Eq. (3.15) is derived in order to produce output states that are stable against the change of an arbitrary parameter a. For the particle-like states investigated so far, this parameter is the frequency ω, however, in the next section we show that we get very promising scattering states if this parameter a is the displacement δ of a scatterer (located in the scattering region) from its center position along a chosen direction $\vec{e}_\delta$, i.e., $q_a = q_\delta$.

3.5 Avoiding and Focusing on a Target using Eigenstates of q_δ

As derived in section 3.3, eigenstates of the operator q_a are stable to first order against the change of an arbitrary parameter a. Assuming that we have a waveguide system with one single scatterer inside the scattering region as shown in Fig. 3.8(a), we now choose this parameter a to be the displacement δ of a scatterer from its center position $\vec{r}_0$ along a certain direction $\vec{e}_\delta = (e_x, e_y)^T$ (represented by a unit vector, i.e., $|\vec{e}_\delta| = 1$), instead of the frequency ω of the incident wave, as we did in the previous section to get particle-like states. Using these parameters, the position of the scatterer $\vec{r}_s$ can be written as a function of the displacement, $\vec{r}_s = \vec{r}_0 + \delta\vec{e}_\delta$. Conducting an experiment, the operator

$$q_\delta = -jt^{-1}\frac{dt}{d\delta} \tag{3.30}$$

can be calculated by a finite but small shift $\Delta\delta$ of the scatterer around the center position $\vec{r}_0$ along direction $\vec{e}_\delta$ accompanied by the measurement of the transmission matrix $t(\delta)$ for every position of the scatterer. In a first step, we calculate eigenstates of q_δ for a change of the position of the scatterer in longitudinal direction (see Fig. 3.8(a)) of the waveguide, i.e., $\vec{e}_\delta = (1, 0)^T$, and for reasons of simplicity we call this operator q_x. Among the eigenstates of q_x, we find a state that has a non-zero wave function in the whole scattering region except in the vicinity of the scatterer, where the wave function is negligible small, as can be seen in Fig. 3.8(b). Also the opposite effect can be observed: one eigenstate of q_x focuses on the scatterer and thus gets reflected entirely, see Fig. 3.8(c). In order to understand this behavior, we go one step back and first try to understand the working mechanism of the operator

$$Q_\delta = -jS^\dagger\frac{dS}{d\delta}, \tag{3.31}$$

which is the corresponding generalization of the Wigner-Smith time-delay operator (3.8). In what follows, we derive a mathematical expression for the eigenvalues of this new operator Q_δ and try to give it a physical interpretation, in analogy to the relation of the Wigner-Smith operator to the delay time.

First we consider an unspecified scattering system, where the whole scattering region is shifted in an arbitrary direction $\vec{e}_\delta$. Since the shift of the system should be small, one can approximate the derivative in Eq. (3.31) by

$$\frac{dS(\delta)}{d\delta} \approx \frac{S(\vec{r}_0 + \Delta\delta\vec{e}_\delta) - S(\vec{r}_0)}{\Delta\delta}. \tag{3.32}$$

The scattering matrix evaluated at the shifted position $S(\vec{r}_0 + \Delta\delta\vec{e}_\delta)$ is related to the scattering matrix at position $\vec{r}_0$, $S(\vec{r}_0)$, by the unitary translation operator

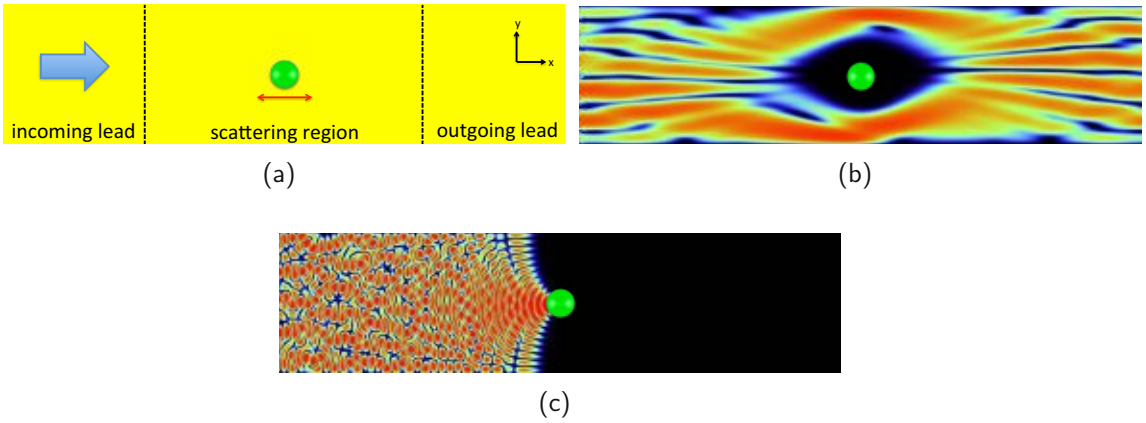

Figure 3.8: (a) Waveguide with one single circular metallic scatterer (green) of which the position is changed in longitudinal direction in order to calculate eigenstates of q_x. (b) Eigenstate of q_x that avoids the scatterer, whereas (c) shows an eigenstate with strong focus on the scatterer. The q_x-eigenvalues were calculated according to Eq. (3.24), where all singular values in the projection of the transmission matrix were used for the calculation. The incoming wavelength allows for a total number of 20 open modes.

$\hat{T} = e^{-j\vec{k}\vec{e}_\delta \Delta\delta}$,

$$S(\vec{r}_0 + \Delta\delta\vec{e}_\delta) = \hat{T}S(\vec{r}_0)\hat{T}^{-1} = e^{-j\vec{k}\vec{e}_\delta\Delta\delta}S(\vec{r}_0)e^{j\vec{k}\vec{e}_\delta\Delta\delta} = e^{-j\hat{k}_e\Delta\delta}S(\vec{r}_0)e^{j\hat{k}_e\Delta\delta}, \quad (3.33)$$

with $\vec{k} = -j\vec{\nabla} = (\hat{k}_x, \hat{k}_y)^T$ and the short notation $\hat{k}_e := \vec{k}\vec{e}_\delta = e_x\hat{k}_x + e_y\hat{k}_y$. For systems with the same number of open modes in both leads, $\hat{k}_x$ and $\hat{k}_y$ take the block form

$$\hat{k}_x = \begin{pmatrix} \hat{k}_x^l & 0 \\ 0 & \hat{k}_x^r \end{pmatrix} \quad (3.34)$$

and

$$\hat{k}_y = \begin{pmatrix} \hat{k}_y^l & 0 \\ 0 & \hat{k}_y^r \end{pmatrix}, \quad (3.35)$$

where $\hat{k}_x^l$ and $\hat{k}_y^l$ are operators acting on the waves in the left-hand lead, i.e., on $\vec{\phi}_l$ and $\vec{\mu}_l$, and $\hat{k}_x^r$ and $\hat{k}_y^r$ acting on $\vec{\phi}_r$ and $\vec{\mu}_r$. The matrix elements of the operator $\hat{k}_y^l = \hat{k}_y^r$, for example, take the explicit form

$$(\hat{k}_y^l)_{mn} = -j\,\langle\chi_m|\frac{d}{dy}|\chi_n\rangle = -j\int_0^W \chi_m(\frac{d}{dy}\chi_n)dy, \quad (3.36)$$

where χ_n are the transverse mode profiles (3.3).

Making again use of the fact that the shift δ is small, one can linearize the exponential term, $e^{j\hat{k}_e\Delta\delta} \approx 1 + j\hat{k}_e\Delta\delta$. Using these expressions, we end up with

$$Q_\delta = -jS^\dagger \frac{dS(\delta)}{d\delta} \tag{3.37}$$

$$= -jS^\dagger \frac{(1 - j\hat{k}_e\Delta\delta)S(\delta)(1 + j\hat{k}_e\Delta\delta) - S(\delta)}{\Delta\delta} \tag{3.38}$$

$$= \hat{k}_e - S^\dagger \hat{k}_e S, \tag{3.39}$$

where we use the unitarity $S^\dagger S = \mathbb{1}$ and neglect the term proportional to $\Delta\delta^2$. The expectation value $\langle Q_\delta \rangle$ for an arbitrary input state $\vec{\phi}$ yields

$$\langle\phi|Q_\delta|\phi\rangle = \vec{\phi}^\dagger Q_\delta \vec{\phi} = \vec{\phi}^\dagger \hat{k}_e \vec{\phi} - \vec{\phi}^\dagger S^\dagger \hat{k}_e S \vec{\phi} = \vec{\phi}^\dagger \hat{k}_e \vec{\phi} - \vec{\mu}^\dagger \hat{k}_e \vec{\mu} = \langle \hat{k}_e \rangle_\phi - \langle \hat{k}_e \rangle_\mu, \tag{3.40}$$

which is the difference between the expectation value of $\hat{k}_e$ of the input state $\vec{\phi}$ and the output state $\vec{\mu} = S\vec{\phi}$. Since the coefficient vectors $\vec{\phi}$ and $\vec{\mu}$ contain the respective flux amplitudes, calculating the expectation value of the operator $\hat{k}_e$ for, e.g., an input vector $\vec{\phi}$, $\phi^\dagger \hat{k}_e \phi$, yields the expectation value for the flux amplitudes rather than the expectation value of the wave amplitudes. However, for reasons of simplicity, we refer to the expectation value $\langle \hat{k}_e \rangle$ as the momentum of $\vec{\phi}$ parallel to $\vec{e}_\delta$, while keeping in mind that this quantity is not exactly equal to the physical momentum. Eq. (3.40) thus provides us with the information of the momentum difference parallel to $\vec{e}_\delta$ between the input and the output state, which is equivalent to the momentum transferred to the system (up to a minus sign).

Now we can go back to our original system with the single scatterer in Fig. 3.8: Shifting a single scatterer in longitudinal direction (x-direction), which in this case is equivalent to shifting the entire scattering region, the expectation value of an arbitrary scattering state $\vec{\phi}$ would correspond to the momentum change in x-direction of this state that is caused by the scatterer. Just as the eigenstates of the Wigner-Smith operator have well-defined delay times, eigenstates of Q_δ have a well-defined momentum transfer. Eigenstates of Q_δ that have an eigenvalue close to zero, i.e., have no change of the momentum in x-direction, are thus states that avoid the scatterer. On the other hand, eigenstates with a large eigenvalue experience a large change of the momentum, and are thus strongly scattered at the obstacle. Hence, by looking at the eigenvalues of Q_δ, we can predict if a state avoids or focuses on the scatterer. Now that we are able to describe the behavior of the new operator Q_δ, we can also explain the eigenstates of q_x in Fig. 3.8(b) and 3.8(c), since the eigenvalues of Q_δ and the real part of the eigenvalues of q_δ are both proportional to the derivative of the scattering phase. The first eigenstate in Fig. 3.8(b) corresponds to an eigenvalue with a small real part and, therefore, avoids the scatterer, whereas the other eigenstate with large real part of the eigenvalue gets strongly scattered.

Until now, we have only discussed the case where the scatterer is shifted in longitudinal direction, which is equivalent to fixing the position of the scatterer and shifting the whole scattering region in x-direction. Shifting the scatterer in transverse direction, however, cannot be seen as shifting the whole scattering region in y-direction by simultaneously fixing the position of the scatterer. The assumption that the scattering matrix of the system with the scatterer at the shifted position, $S(\vec{r}_0 + \Delta\delta\vec{e}_\delta)$, is related to the scattering matrix of the system where the scatterer is at its center position, $S(\vec{r}_0)$, by a translation operator $\hat{T}$ is thus not valid and the eigenvalues of (3.31) cannot be interpreted as the momentum difference between input and output state anymore. However, we show in the following paragraph that (at least) for the investigated system there is a correlation between the eigenvalues of the operator and the momentum difference of input and output state also for the case where the scatterer is shifted in y-direction, although this is not yet completely understood. Therefore, we assume in the following that in both cases (transverse and longitudinal shifting of the scatterer) the eigenvalues yield the momentum difference in a chosen direction between input and output state.

Contrary to the eigenvalues of the Wigner-Smith time-delay operator, eigenvalues of Q_δ and q_δ can also be negative, since the momentum is a signed quantity. We now show how we can make use of this fact in order to characterize the scattering states in more detail. Assume again, that there is only one single scatterer inside the system. The real part of the eigenvalue of q_δ is proportional to the momentum difference (parallel to a chosen direction) between input and output state. Due to momentum-conservation, the same momentum (but opposite sign) had to be transferred to the scatterer (apart from scattering at the boundary, which is subject of current investigations). The sign of the eigenvalue is therefore directly related to the direction from which the wave focuses on the scatterer, just as a particle hits a target from a certain direction. We illustrate this issue by showing two systems: In Fig. 3.9(a) we can see a waveguide system with one quadratic scatterer located in the middle. In this system, the operator q_δ will be calculated by changing the position of the scatterer in longitudinal direction x (i.e., $q_\delta = q_x$), whereas in the system shown in Fig. 3.9(b), the scatterer is shifted in transverse direction y (i.e., $q_\delta = q_y$). Figs. 3.9(c) and 3.9(d) show the q_x- and q_y-eigenstate with the smallest eigenvalue of either system shown in 3.9(a) and 3.9(b), respectively, where we can clearly see that the wave functions of both states pass by the scatterer. Now comes the crucial difference: In Fig. 3.9(e) and Fig. 3.9(g) we can see two q_x-eigenstates with the highest real parts of the eigenvalues τ_x. Both eigenvalues have the same sign and are of the same order of magnitude, since they correspond to scattering states that are mirror-symmetric to each other. Fig. 3.9(f) and Fig. 3.9(h) show two eigenstates of q_y with the highest real parts of the eigenvalues τ_y which are mirror-symmetric to each other as well, but the eigenvalues have opposite signs. This stems from the fact that the operator q_y measures the momentum difference in y-direction, which is obviously different for those states. The momentum-difference in x-direction,

however, is almost the same, which explains the same sign of the eigenvalues of the eigenstates of q_x. The connection between the sign and the eigenvalues is valid for all eigenstates of q_y and not only for the ones shown here. Thus, one can predict the side from which the wave impinges onto the obstacle relative to the direction in which the scatterer is shifted, however, if there are more scatterers in the system, this connection between the eigenvalues and the wave function is not valid anymore due to multiple scattering. In the next subsection we discuss an experimental realization of such avoiding and focusing states in a microwave set-up and show first experimental results from the experiment conducted at the University of Nice.

3.5.1 Avoiding and Focusing on a Target in the Experiment

In order to show that the focusing and avoiding mechanism works also in a strongly scattering environment, additional cylindrical scatterers are placed inside the scattering region around the main scatterer that should be avoided and focused on, respectively, as can be seen in Fig. 3.10(a). The main scatterer is a metallic cylinder which is located in the middle of the scattering region and the randomly distributed smaller scatterers are teflon cylinders with a refractive index of $n = 1.44$. The lead width $W = 10$ cm and 10 antennas working at a frequency of $\nu = 15.5$ GHz support a total number of 10 flux-carrying modes.

The task is now to choose the relevant eigenstates (those that avoid or focus on the main scatterer) among the $10 + 9 + 8 + ... + 1 = 55$ eigenstates that we get for every possible singular value decomposition in the calculation of q_δ in Eq. (3.24) without looking at the wave function of the scattering state. The question of identifying the relevant eigenstates on the basis of quantities that are available in the asymptotic regions is of fundamental importance, since for real applications, the scattering region is not always accessible (e.g. in human tissue). A state that avoids the scatterer is characterized by a small real part of the eigenvalue τ_δ. Among those states there are also states that get reflected at the smaller scatterers at the front facet of the scattering region and thus feature a small transmission. If we want to sort out those states, we can demand, besides a small real part of τ_δ, also a high transmittance T_ϕ of the state $\vec{\phi}_l$, which is given by $T_\phi = |t\vec{\phi}_l|^2$, where t is the measured transmission matrix. The imaginary part of τ_δ tells us how the total output intensity changes as a function of the position of the scatterer. Since the output intensity of avoiding states should not be affected by a small change of the position, the imaginary part of τ_δ should be small for those states. Using the criterion

$$\kappa = \frac{|\tau_\delta|}{|T_\phi|} \tag{3.41}$$

in order to sort all 55 possible eigenstates, we can find the "best" avoiding scattering states among the eigenstates with the smallest value κ. On the other hand,

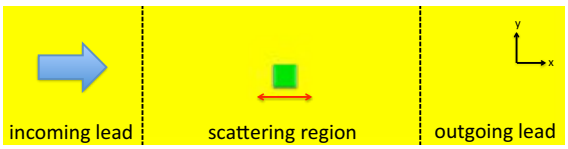

(a) Waveguide with one quadratic scatterer that is shifted in longitudinal direction in order to calculate the operator $q_{r=x}$.

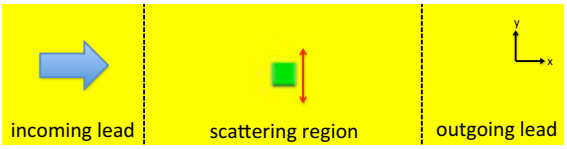

(b) Waveguide with one quadratic scatterer that is shifted in transverse direction in order to calculate the operator $q_{r=y}$.

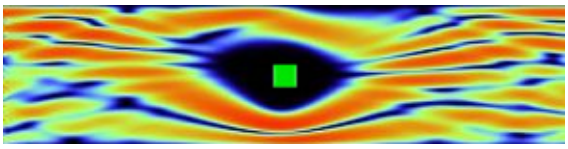

(c) q_x-eigenstate with the smallest real part of the eigenvalue, $\mathrm{Re}(\tau_x) = 2.059 \times 10^{-12}$

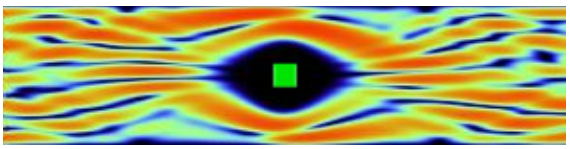

(d) q_y-eigenstate with the smallest real part of the eigenvalue, $\mathrm{Re}(\tau_y) = 4.022 \times 10^{-14}$

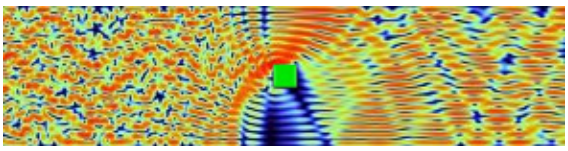

(e) q_x-eigenstate with large positive real part of the eigenvalue, $\mathrm{Re}(\tau_x) = 0.07961$

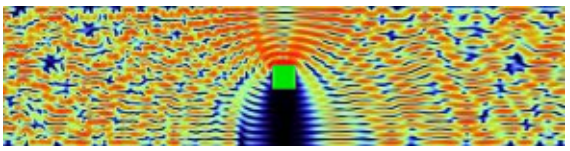

(f) q_y-eigenstate with large real part of the eigenvalue, $\mathrm{Re}(\tau_y) = 0.7153$

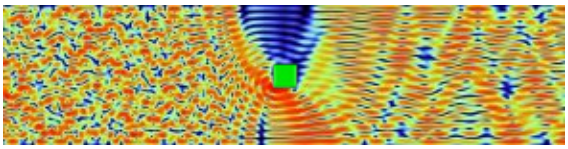

(g) q_x-eigenstate with large real part of the eigenvalue, $\mathrm{Re}(\tau_x) = 0.1072$

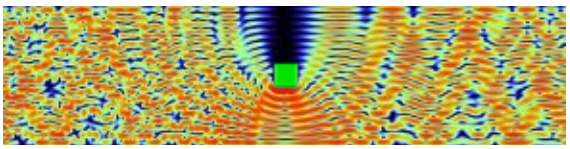

(h) q_y-eigenstate with large negative real part of the eigenvalue, $\mathrm{Re}(\tau_y) = -0.8039$

Figure 3.9: The left column shows the waveguide system with q_x-eigenstates, in which the scatterer (green) is shifted in longitudinal direction (x), whereas the right column shows the same results for transverse (y) shifting of the scatterer. The sign of the real part of the eigenvalues of q_y determines whether the state hits the obstacle from the top or from the bottom, since q_y measures the momentum difference in y direction. Since all q_x-eigenstates hit the obstacle from the left-hand side, all eigenvalues have the same (positive) sign. The $q_{x,y}$-eigenstates were calculated according to Eq. (3.24), where the four smallest singular values were neglected. The chosen value of the incoming wavelength results in a total number of 20 propagating modes.

eigenstates that focus onto the main scatterer have a large real part of τ_δ and a large imaginary part of τ_δ, since the output intensity of the focusing states could change significantly when the position of the scatterer is changed. The "best" focusing states can thus be found among the eigenstates that have a large eigenvalue $|\tau_\delta|$. Including the transmittance T_ϕ of the eigenstates into the selection process for focusing states, like in criterion (3.41), is not practical since states that get reflected at the smaller background scatterer feature a small transmittance as well without being scattered at the main scatterer.

In collaboration with the University of Nice we calculated all 55 q_δ-eigenstates for a shift of the main scatterer in transverse direction, $q_\delta = q_y$, and sorted them by the criterion (3.41) and the eigenvalue $|\tau_\delta|$, respectively, in a real microwave set-up. In Fig. 3.10(b)-3.10(g) we can see three q_y-eigenstates with the smallest κ-value and three eigenstates with the largest eigenvalue $|\tau_\delta|$, respectively. Whereas the states with the smallest κ-value show a low intensity in the vicinity of the main scatterer, the states with the highest eigenvalue show a strong focus, which is in very good agreement with our theory.

At this point we want to emphasize that these results open up a new and promising way of wave front shaping experiments. Focusing on a target inside a scattering medium has already been realized experimentally [49–52], however, our approach derives from novel solid, theoretical grounds. A completely new approach is the omission of a target inside a scattering medium. Both strategies can lead to new and useful applications ranging from medical radiotherapy (destroying a tumor through wave focusing or the omission of healthy organs) to wireless communication (where the focus should be maintained on a mobile receiver). We think that this first successful experiment, which proves our theory, is just the beginning of a new direction in the domain of wave front control.

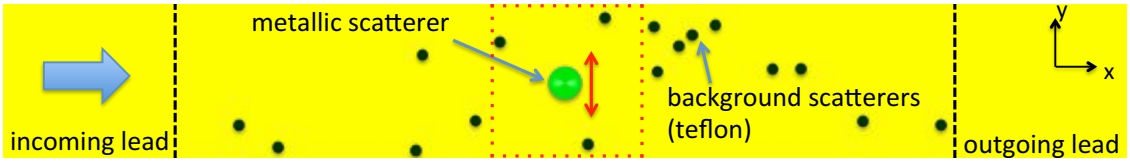

(a) Sketch of the experimental set-up: waveguide with a width of $W = 10$ cm. The metallic main scatterer (light green, diameter $d = 17.65$ mm) is shifted in transverse direction in order to calculate q_y-eigenstates. The smaller background scatterer (dark green) are made of teflon ($n = 1.44$) and have a diameter of $d = 5.1$ mm. 10 antennas working at a frequency of $\nu = 15.5$ GHz allow for a total number of 10 flux-carrying modes. The positions of the background scatterers is different in the real experiment. The red dotted lines indicate the region which is shown in the plots below.

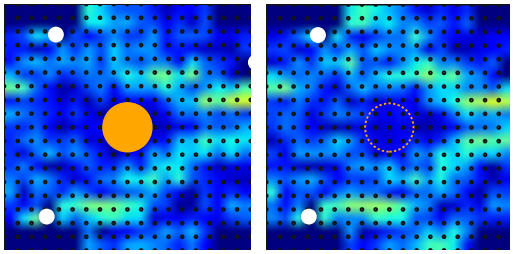

(b) $n_\epsilon = 8$, $\kappa = 0.00499$

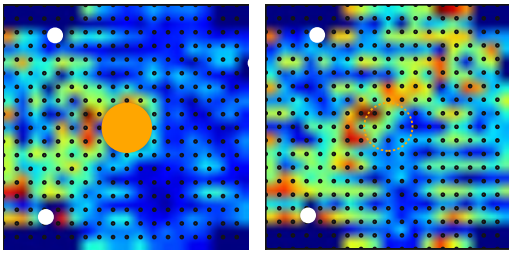

(c) $n_\epsilon = 9$, $|\tau_\delta| = 0.713$

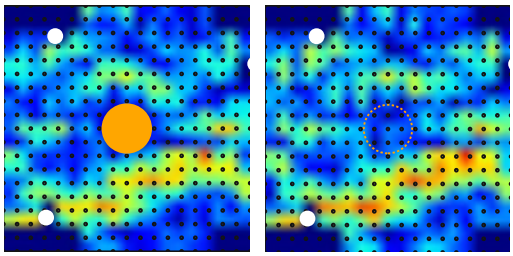

(d) $n_\epsilon = 5$, $\kappa = 0.0063$

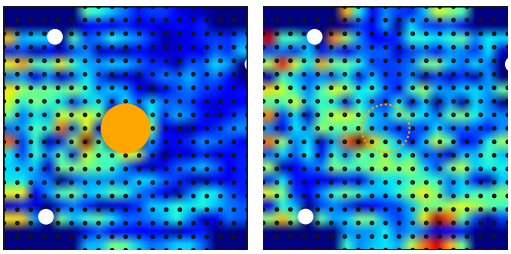

(e) $n_\epsilon = 10$, $|\tau_\delta| = 0.934$

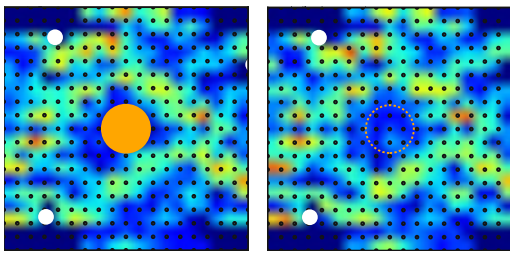

(f) $n_\epsilon = 3$, $\kappa = 0.00631$

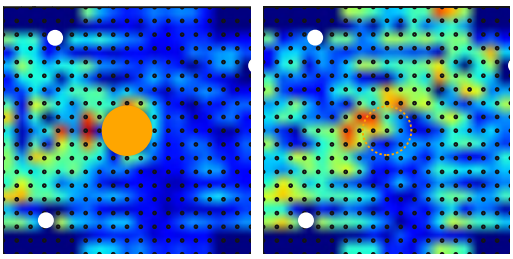

(g) $n_\epsilon = 10$, $|\tau_\delta| = 1$

Figure 3.10: The left column shows three experimentally measured q_y-eigenstates that have the smallest κ-value (normalized by the highest value) as defined in Eq. (3.41) with (left) and without main scatterer (right) inside the system. The wave function shows a significant drop around the scatterer and thus changes barely when the scatterer is taken out. The eigenstates with the highest eigenvalues $|\tau_\delta|$ (normalized by the highest value) are shown in the right column and clearly focus onto the metallic scatterer, thus changing significantly when the scatterer is removed. n_ϵ is the number of singular values that will be used for the projection in Eq. (3.24). The intensity plots show only the region around the main scatterer indicated by the red dotted lines in (a). The main scatterer is shifted by $\Delta\delta \approx 4.4$ mm in order to approximate the derivative in q_y by a finite difference quotient.

3.6 Coherent Perfect Absorber (CPA)

One important milestone in modern physics was the invention of the laser. In its most simple form, a laser consists of an amplifying medium that is placed inside a resonator and, under specific conditions, starts to emit coherent monochromatic radiation. Going now to arbitrary scattering systems, one can calculate poles and zeros of its scattering matrix S in the extended complex k-plane. Whereas in Hermitian systems zeros are located in the upper half of the complex k-plane (where $\mathrm{Im}(k) > 0$), poles are located in the lower k-plane ($\mathrm{Im(k)} < 0$). Adding gain to the system moves the poles up towards the real k-axis where the system turns into a laser when a pole crosses the real k-axis. The opposite is also possible: adding loss to a system moves down the zeros until one reaches the real k-axis. Injecting an eigenvector of the S-matrix with eigenvalue equal to zero into this scattering system leads to a vanishing outgoing wave, i.e., perfect absorption of the incoming wave. This phenomenon is the time-reversed process of a laser and referred to as a coherent perfect absorber (CPA) [24]. Considering a two-dimensional waveguide system, where a wave can be injected from both sides, a physical interpretation of a CPA can be given as follows: The reflected part of the wave injected from the left-hand lead destructively interferes with the transmitted part of the wave injected from the right-hand lead and vice versa. The intensity is therefore ”trapped” inside the scattering region due to interference, where the lossy medium will absorb the wave completely. The term ”coherent” comes from the fact that the relative phase between the right-hand and left-hand injected wave has to be tuned in order to end up with the required interference pattern.

Whereas in conventional laser systems a resonator plays an essential part, so-called random lasers are based on a different working mechanism: a disordered gain medium leads to multiple scattering of light which increases the path length inside the gain medium and thus enhances amplification [53]. The time-reversed process of a conventional laser (“anti-laser”) has already been realized experimentally [25, 26], however, the time reversed process of a random laser (“anti-random laser”) has defied an experimental realization so far.

In the next subsection we discuss all the steps that are necessary in order to prove that a two-dimensional waveguide system with randomly distributed scatterers inside the scattering region is at a CPA point (and in this way acts as an “anti-random laser”) with strong focus on an experimental realization with microwaves.

3.6.1 Possible Experimental Realization of a CPA

Contrary to the systems we used before, a CPA requires injection from both sides of the scattering region, i.e., antennas on the right-hand side and antennas on the left-hand side will inject radiation into the system, as can be seen in Fig. 3.11. The absorbing material will be represented by a passive antenna in the middle

of the scattering region that leads to an outcoupling of intensity and, therefore, introduces loss. The CPA point is achieved when the entire incoming radiation is coupled into this antenna inside the scattering region. Since a certain degree of outcoupling and absorption due to other mechanisms is always present in a real system, the energy coupled to the absorber antenna will be less than the energy injected into the system, which makes it hard to prove that the system has reached the CPA point. Therefore, claiming that the system has reached the CPA point following an argument based on energy conservation is difficult. In the following, we present a method that enables us to measure the full scattering matrix S, i.e., the transmission matrices t_l and t_r as well as the reflection matrices r_l and r_r, with the aim of finding the CPA point by calculating zeros of the scattering matrix S. This condition is sufficient to prove that the injected intensity is maximally coupled to the absorbing antenna, which thus acts as a perfect absorber.

As already mentioned in the previous sections, measuring the reflection matrices (r_l and r_r) is hard to do in experiments, however, additional measurements of the wave on either side of the scattering region, enables a full measurement of the scattering matrix S. Fig. 3.11 shows the complete set-up of the CPA experiment, where antenna arrays $A1$ and $A2$ are those antennas that will inject radiation into the system, whereas the two double antenna arrays $P1$ and $P2$ will only be used as a probe to measure the wave function, so that we refer to them as probe antennas. In practice, $P1$ and $P2$ do not have to be independent fixed antennas but can rather be positions where a movable antenna can be placed, however, for reasons of simplicity, we assume that we have separate antennas. $A1$ and $A2$ are separated by a distance L, whereas the distance between $A1$ and $P1$, as well as between $A2$ and $P2$ is L_0. The absorbing antenna, which is used instead of a lossy material, is labeled as A_a and furthermore, cylindrical scatterers are placed inside the scattering region to increase multiple scattering, which is an essential part of an "anti-random laser".

Absorption inside the waveguide leads to complex propagation constants, $\beta_n = k_{x,n} + i\gamma_n$ for right-propagating waves and β_n^* for left-propagating waves, where $\gamma_n > 0$ is the absorption coefficient and $k_{x,n}$ is the wavenumber in longitudinal direction of the n-th mode. An arbitrary signal σ_m measured at the m-th antenna of $P1$ at transverse position y_m can be written as

$$\begin{aligned}\sigma_m(L_0) = \sigma(x = L_0, y = y_m) &= \sum_{n=1}^{N} [a_n e^{j\beta_n L_0} + b_n e^{-j\beta_n^* L_0}]\chi_n(y_m) \\ &= \sum_{n=1}^{N} [a_n e^{jk_{x,n}L_0} e^{-\gamma_n L_0} + b_n e^{-jk_{x,n}L_0} e^{-\gamma_n L_0}]\chi_n(y_m)\end{aligned} \tag{3.42}$$

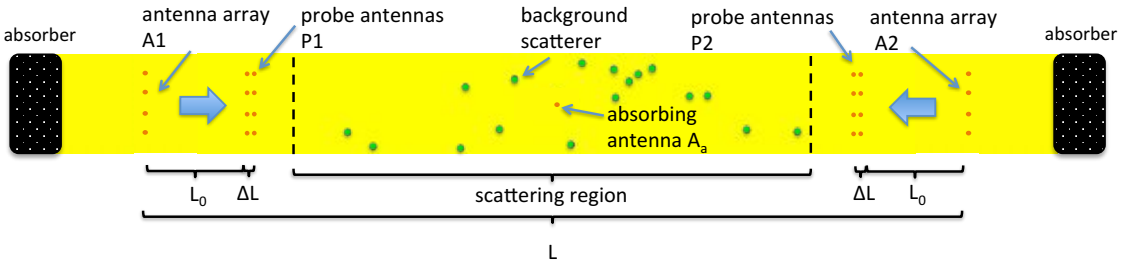

Figure 3.11: Sketch of the set-up for the CPA experiment. Antenna array $A1$ and $A2$ will inject an eigenstate that corresponds to a zero of the scattering matrix S. This state gets fully absorbed at the absorbing antenna A_a in the middle of the scattering region. Probe antennas $P1$ and $P2$ are used to calculate the reflection matrices r_r and r_l. Randomly distributed scatterers (green) are placed inside the scattering region to increase scattering within the system. Absorbers are placed at the ends of the scattering geometry to avoid reflections at the open end of the waveguide. The incoming wavelength is chosen in such a way, that four modes are open at either side of the waveguide outside the scattering region.

and

$$\begin{aligned}\sigma_m(L_0+\Delta L) &= \sum_{n=1}^{N}[a_n e^{j\beta_n(L_0+\Delta L)} + b_n e^{-j\beta_n^*(L_0+\Delta L)}]\chi_n(y_m) \\ &= \sum_{n=1}^{N}[a_n e^{jk_{x,n}(L_0+\Delta L)}e^{-\gamma_n(L_0+\Delta L)} \\ &\qquad + b_n e^{-jk_{x,n}(L_0+\Delta L)}e^{-\gamma_n(L_0+\Delta L)}]\chi_n(y_m),\end{aligned} \tag{3.43}$$

where N is the number of open modes, $\chi_n(y)$ is the transverse lead-mode profile of the n-th mode as given in Eq. (3.3) and a_n and b_n are arbitrary complex coefficients. The signals $\sigma_m(L-L_0)$ and $\sigma_m(L-(L_0+\Delta L))$ for the probe antennas $P2$ can be written in analogy to the above equations, but with different complex coefficients c_n and d_n. In a first step, we determine the complex propagation constants β_n with an empty measurement set-up, i.e., without absorbing antenna A_a and without scatterers. Although the system is empty, the absorbers at the end of the system will cause small reflections, but no mode mixing. Injecting the n-th mode from the left lead, we can measure the signals $\sigma_n^l(x,y_m) = \sigma_{n,m}^l(x)$ at the m-th probe antenna of $P1$

$$\begin{aligned}\sigma_{n,m}^l(L_0) &= e^{j\beta_n L_0}\chi_n(y_m) + \tilde{r}_{nn}^l e^{-j\beta_n^* L_0}\chi_n(y_m), \\ \sigma_{n,m}^l(L_0+\Delta L) &= e^{j\beta_n(L_0+\Delta L)}\chi_n(y_m) + \tilde{r}_{nn}^l e^{-j\beta_n^*(L_0+\Delta L)}\chi_n(y_m),\end{aligned} \tag{3.44}$$

where $\tilde{r}^l_{nn}$ is the n-th diagonal element of the (diagonal) reflection matrix $\tilde{r}_l$ of the empty system. For N flux-carrying channels, we have to determine N complex propagation constants β_n and N complex reflection matrix elements $\tilde{r}_{nn}$, i.e., $2N$ complex quantities, which requires $2N$ linearly independent complex equations. These equations can be obtained from the measurement of the signals (3.44) at one transverse position y_m but at two longitudinal positions L_0 and $L_0 + \Delta L$ for each mode. The measurement of the signals at every transverse position y_m and the measurement of the signals at antenna array $P2$ for injection from the right-hand side are redundant, however, those additional measurements can be used for a more precise determination of the propagation constants β_n. The calculated propagation constants β_n can be verified by measuring the transmission matrices t_r and t_l between the antenna arrays $A1$ and $A2$ which take the easy form $t_l = t_r^* = \mathrm{diag}(\mathrm{e}^{\mathrm{j}\beta_\mathrm{n}\mathrm{L}})$ in an empty system. Now that we have determined the propagation constants β_n, we can measure the reflection matrices $\tilde{r}_r$ and $\tilde{r}_l$ of the scattering system with absorbing antenna A_a and the scatterers put in place in a second step. Analogous to Eq. (3.44), we can measure the signals at antenna array $P1$ for injection of the n-th mode

$$\sigma^l_{n,m}(L_0) = e^{j\beta_n L_0}\chi_n(y_m) + \sum_{i=1}^{N} \tilde{r}^l_{ni} e^{-j\beta_i^* L_0}\chi_n(y_m). \tag{3.45}$$

Contrary to the empty system, the reflection matrix $\tilde{r}_l$ now has $N \times N$ non-zero elements, which requires the measurement of the signals at all N transverse positions, $(y_m, m = 1, ...N)$ for each of the N injected modes to get N^2 equations. Eq. (3.45) can be written in matrix form as

$$\Sigma = B^+ \cdot C + r_l \cdot B^- \cdot C, \tag{3.46}$$

with $(\Sigma)_{nm} = \sigma^l_{n,m}(L_0)$, $(B^\pm)_{nl} = e^{\pm j\beta_n L_0}\delta_{nl}$ and $(C)_{lm} = \chi_l(y_m)$, where δ_{nl} denotes the Kronecker-delta. Solving for the reflection matrix $\tilde{r}_l$, we end up with

$$\tilde{r}_l = (\Sigma - B^+ \cdot C) \cdot (B^- \cdot C)^{-1}. \tag{3.47}$$

The reflection matrix $\tilde{r}_r$ can be calculated in analogy to Eq. (3.46) by measuring the signals at $P2$ for injection from the right-hand antenna array $A2$. Due to time-reversal symmetry, $\tilde{r}_l = \tilde{r}_l^T$ and $\tilde{r}_r = \tilde{r}_r^T$, there are less than N^2 independent entries of $\tilde{r}_l$ and $\tilde{r}_r$ providing a possibility to verify the results. Since we use the signal at the probe antennas $P1$ and $P2$ for our calculations, we actually determine the reflection matrices for the reduced system between the antenna arrays $P1$ and $P2$ rather than the reflection matrices of the full system between $A1$ and $A2$. The full reflection matrices r_l and r_r can then be calculated according to

$$r_l = t_{AP} \cdot \tilde{r}_l \cdot t_{AP} \tag{3.48}$$

$$r_r = t'_{AP} \cdot \tilde{r}_r \cdot t'_{AP}, \tag{3.49}$$

where $t_{AP} = (t'_{AP})^* = \mathrm{diag}(e^{j\beta_n L_0})$ are the transmission matrices between $A1$ and $P1$ as well as $A2$ and $P2$, which can be measured in the empty set-up in a previous step. In a last step, we have to measure the transmission matrices t_l and t_r between $A1$ and $A2$ so that we have the information of the full scattering matrix in the usual form

$$S = \begin{pmatrix} r_l & t_r \\ t_l & r_r \end{pmatrix}. \tag{3.50}$$

This procedure will be performed for each frequency ν in an interval $\Delta\nu$ by simultaneously calculating the $2N$ eigenvalues $\lambda_n(\nu)$ of $S(\nu)$. If one eigenvalue becomes zero at a certain frequency ν_{CPA}, the corresponding eigenvector $\vec{\phi} = (\vec{\phi}_l,\ \vec{\phi}_r)^T$ contains the information on how to adjust the relative phases and amplitudes of the antennas in $A1$, $\vec{\phi}_l$, and $A2$, $\vec{\phi}_r$, in order to achieve perfect absorption of the incident wave. At this point, the injected wave is maximally coupled to antenna A_a. Using an antenna as the dissipative element of the CPA brings one big advantage: We can verify that the injected wave is maximally absorbed by the antenna A_a by calculating the transmission matrix from antennas $A1$ and $A2$ to the absorber antenna A_a. This $1 \times 2N$-dimensional transmission matrix t can be used to calculate eigenvectors of the $2N \times 2N$-dimensional matrix $t^\dagger t$. The eigenvector of $t^\dagger t$ with the highest eigenvalue, i.e., with the highest transmittance to the antenna A_a, has to coincide with the eigenvector $\vec{\phi}$ of the previously calculated scattering matrix S with eigenvalue zero.

To summarize, in this section we develop an algorithm that can be used to find a CPA point in a dissipative and disordered two-port waveguide system - a so-called "anti-random laser" - by considering experimental constraints. The corresponding experiment at the University of Nice with $N = 4$ antennas in each of the two antenna array (and $N = 4$ flux-carrying modes) is currently in preparation. The encouraging results of the microwave experiments mentioned before let us expect that also this experiment will yield a positive outcome.

Chapter 4

Conclusion

In this thesis we present two opposing approaches for controlling the propagation of waves in specific geometries. The first approach deals with the control of waves by manipulating the scattering medium itself. We show that a proper design of a material's refractive index can lead to constant-intensity waves [19]. One of the main results of this thesis is the explanation of the working mechanism of these waves in systems, in which the refractive index varies in propagation direction. We show that constant-intensity waves are the non-Hermitian analogue to plane waves in Hermitian systems without any back reflections in the entire system.

Constant-intensity waves have a number of interesting properties. Due to the special form of CI refractive indices, the connection to supersymmetric quantum mechanics is investigated. We show, that constant-intensity waves can alternatively be derived in the framework of supersymmetric quantum mechanics by demanding that the superpotential has to be purely imaginary. Also, a relation to $\mathcal{PT}$-symmetry is shown. Most strikingly, however, is the fact that some constant-intensity refractive indices can be unidirectionally invisible. The unidirectionally invisible refractive index in the well-established work [22] is just one example of a whole class of unidirectionally invisible CI refractive indices introduced in this thesis.

By generalizing the concept of constant-intensity waves, we find that not only the phase, but also the amplitude (as a function of the spatial coordinate) of the scattering state can be predetermined by correctly tailoring the complex refractive index, leading to a new class of reflectionless refractive index distributions. These refractive indices can be calculated analytically from the desired form (amplitude and phase) of the scattering wave function.

After these theoretical considerations, we also discuss two possible experimental realizations of constant-intensity waves without the difficulty of implementing gain regions. Whereas one possible experiment would show a true constant-intensity wave, the second one leads to a uniformly decaying wave function, but still shows the concept of constant-intensity waves.

In the second part of this thesis we show that we can achieve certain aspects of wave control by changing the incident wave front rather than the medium itself.

Inspired by the Wigner-Smith time-delay operator Q_ω, we introduce a whole new operator class that can be constructed from the transmission matrix t exclusively and has the useful feature of producing scattering states that are stable against the change of an arbitrary parameter. One example of this class, q_ω, can be used to find scattering states with a beam-like behavior. We analyze all aspects of an experimental realization of such particle-like states in a microwave cavity and also show first promising results from our collaborators from the University of Nice.

Whereas particle-like states are scattering states that are stable against the change of the incident frequency, new wave effects can be observed if this parameter is chosen to be the position of a scatterer located inside a scattering region. Some of the eigenstates of the corresponding operator q_δ either focus onto or omit the scatterer (whose position is changed) in the sense that the wave function is negligibly small around the scatterer. Focusing on a target that is located inside the medium has already been achieved experimentally, however, the presented algorithm is easy to implement and is based on an elegant theoretical concept. The same algorithm can lead to scattering states that avoid a specific scatterer that can even be located in a strongly scattering medium, e.g., randomly distributed background scatterers, which is a completely new approach in wave front shaping. This fascinating feature can lead to useful applications, e.g., in the medical domain. An experiment conducted at the University of Nice demonstrated clearly these new scattering states, thereby confirming our theoretical predictions.

Injecting waves in a disordered two-port waveguide system with a dissipative element can lead to perfect absorption of the incident wave. An experimental realization of such a coherent perfect absorber (CPA) is discussed in the last section. Experimental results are unfortunately not yet available, however, we are expecting a successful outcome since our numerical simulations are in good agreement with the experimental data so far.

All promising numerical as well as experimental results presented in this thesis show in which way wave control can be used to create novel and counterintuitive scattering states. Whereas the wave front shaping predictions are confirmed or are already in a preparatory experimental state, there is no experimental realization of constant-intensity waves yet. A future goal of our work will thus be to make specific predictions for the realization of these exotic wave states in currently available experimental setups.

Acknowledgements

Finally I would like to thank the following people who helped, inspired and encouraged me during the tough but very rewarding time I was working on this thesis:

- My thesis advisor Prof. Dr. Stefan Rotter who gave me the possibility to conduct this thesis in a very professional and well functioning scientific group. He was always open for my questions and took time for discussions even in stressful times. He also put a lot of trust in me by sending me to conferences to present my results thus giving me the opportunity to gain experience.
- My thesis co-advisor Dipl.-Ing. Philipp Ambichl who took a lot of time introducing me to most of the physical concepts which I used in this thesis. He was always willing to help and deepen my understanding of physics.
- Dr. Konstantinos Makris for many interesting and fruitful discussions.
- Prof. Dr. Ulrich Kuhl and his PhD student Julian Böhm from the University of Nice who put a lot of work and effort in realizing the microwave experiments. Our collaboration was very successful and made a lot of fun.
- Dr. Florian Libisch who granted me full access to his computer code and Dr. Adrian Girschik who helped me every time I had problems with it.
- The colleagues in my working group for interesting conversations and their contribution to a pleasant and constructive working atmosphere.

Last but not least I want to thank my family, friends and especially my girlfriend, for their moral support and for creating a healthy balance between my work and my private live.

Bibliography

[1] E. Akkermans and G. Montambaux, *Mesoscopic Physics of Electrons and Photons*. Cambridge University Press, 2007.

[2] P. Sebbah, *Waves and Imaging through complex media*. Kluwer Academic, 1999.

[3] A. P. Mosk, A. Lagendijk, G. Lerosey, and M. Fink, "Controlling waves in space and time for imaging and focusing in complex media," *Nature Photonics*, vol. 6, p. 283, 2012.

[4] I. M. Vellekoop and A. P. Mosk, "Focusing coherent light through opaque strongly scattering media," *Optics Letters*, vol. 32, p. 2309, 2007.

[5] S. M. Popoff, G. Lerosey, R. Carminati, M. Fink, A. C. Boccara, and S. Gigan, "Measuring the Transmission Matrix in Optics: An Approach to the Study and Control of Light Propagation in Disordered Media," *Physical Review Letters*, vol. 104, p. 100601, 2010.

[6] I. M. Vellekoop, A. Lagendijk, and A. P. Mosk, "Exploiting disorder for perfect focusing," *Nature Photonics*, vol. 4, pp. 320–322, 2010.

[7] O. Katz, E. Small, Y. Bromberg, and Y. Silberberg, "Focusing and compression of ultrashort pulses through scattering media," *Nature Photonics*, vol. 5, p. 372, 2011.

[8] D. J. McCabe, A. Tajalli, D. R. Austin, P. Bondareff, I. A. Walmsley, S. Gigan, and B. Chatel, "Spatio-temporal focusing of an ultrafast pulse through a multiply scattering medium," *Nature Communications*, vol. 2, p. 447, 2011.

[9] Z. Yaqoob, D. Psaltis, M. S. Feld, and C. Yang, "Optical phase conjugation for turbidity suppression in biological samples," *Nature Photonics*, vol. 2, no. 2, pp. 110–115, 2008.

[10] F. Riboli, N. Caselli, S. Vignolini, F. Intonti, K. Vynck, P. Barthelemy, A. Gerardino, L. Balet, L. H. Li, A. Fiore, M. Gurioli, and D. S. Wiersma, "Engineering of light confinement in strongly scattering disordered media," *Nature Materials*, vol. 13, no. 7, pp. 720–725, 2014.

[11] S. Rotter, "Random lasers: Playing pinball with light," *Nature Physics*, vol. 10, no. 6, pp. 412–413, 2014.

[12] N. Bachelard, S. Gigan, X. Noblin, and P. Sebbah, "Adaptive pumping for spectral control of random lasers," *Nature Physics*, vol. 10, no. 6, pp. 426–431, 2014.

[13] T. Hisch, M. Liertzer, D. Pogany, F. Mintert, and S. Rotter, "Pump-Controlled Directional Light Emission from Random Lasers," *Physical Review Letters*, vol. 111, no. 2, p. 023902, 2013.

[14] L. Ge, O. Malik, and H. E. Türeci, "Enhancement of laser power-efficiency by control of spatial hole burning interactions," *Nature Photonics*, vol. 8, no. 11, pp. 871–875, 2014.

[15] S. F. Liew, B. Redding, L. Ge, G. S. Solomon, and H. Cao, "Active control of emission directionality of semiconductor microdisk lasers," *Applied Physics Letters*, vol. 104, no. 23, 2014.

[16] J. Pendry, "Photonics: Metamaterials in the sunshine," *Nature Materials*, vol. 5, no. 8, pp. 599–600, 2006.

[17] D. R. Smith, W. J. Padilla, D. C. Vier, S. C. Nemat-Nasser, and S. Schultz, "Composite Medium with Simultaneously Negative Permeability and Permittivity," *Physical Review Letters*, vol. 84, no. 18, pp. 4184–4187, 2000.

[18] K. G. Makris, Z. H. Musslimani, D. N. Christodoulides, and S. Rotter, "Constant-intensity waves and their modulation instability in non-Hermitian potentials," *Nature Communications*, vol. 6, 2015.

[19] K. G. Makris, A. Brandstötter, P. Ambichl, Z. H. Musslimani, and S. Rotter, "Wave Propagation through Disordered Media without Backscattering nor Interference Fringes." under review.

[20] C. M. Bender and S. Boettcher, "Real Spectra in Non-Hermitian Hamiltonians Having PT-Symmetry," *Physical Review Letters*, vol. 80, no. 24, pp. 5243–5246, 1998.

[21] C. M. Bender, D. C. Brody, and H. F. Jones, "Complex Extension of Quantum Mechanics," *Physical Review Letters*, vol. 89, no. 27, p. 270401, 2002.

[22] Z. Lin, H. Ramezani, T. Eichelkraut, T. Kottos, H. Cao, and D. N. Christodoulides, "Unidirectional Invisibility Induced by PT-Symmetric Periodic Structures," *Physical Review Letters*, vol. 106, p. 213901, 2011.

[23] S. Rotter, P. Ambichl, and F. Libisch, "Generating Particlelike Scattering States in Wave Transport," *Physical Review Letters*, vol. 106, p. 120602, 2011.

[24] Y. D. Chong, L. Ge, H. Cao, and A. D. Stone, "Coherent Perfect Absorbers: Time-reversed Lasers," *Physical Review Letters*, vol. 105, p. 53901, 2010.

[25] W. Wan, Y. Chong, L. Ge, H. Noh, A. D. Stone, and H. Cao, "Time-Reversed Lasing and Interferometric Control of Absorption," *Science*, vol. 331, p. 889, 2011.

[26] Y. Sun, W. Tan, H.-Q. Li, J. Li, and H. Chen, "Experimental Demonstration of a Coherent Perfect Absorber with PT Phase Transition," *Physical Review Letters*, vol. 112, p. 143903, 2014.

[27] U. Leonhardt, "Optical conformal mapping," *Science*, vol. 312, no. 5781, pp. 1777–1780, 2006.

[28] R. Tyson, *Principles of Adaptive Optics*. CRC Press, 2010.

[29] N. Moiseyev, *Non-Hermitian Quantum Mechanics*. Cambridge University Press, 2011.

[30] C. M. Bender, "Making sense of non-hermitian hamiltonians," *Reports on Progress in Physics*, vol. 70, no. 6, p. 947, 2007.

[31] P. Yeh, A. Yariv, and C.-S. Hong, "Electromagnetic propagation in periodic stratified media. I. General theory," *Journal of Optical Society of America*, vol. 67, pp. 423–438, 1977.

[32] H.-J. Stöckmann, *Quantum Chaos - An Introduction*. Cambridge University Press, 1999.

[33] M.-A. Miri, M. Heinrich, and D. N. Christodoulides, "Supersymmetry-generated complex optical potentials with real spectra," *Physical Review A*, vol. 87, p. 43819, 2013.

[34] M. Heinrich, M.-A. Miri, S. Stützer, R. El-Ganainy, S. Nolte, A. Szameit, and D. N. Christodoulides, "Supersymmetric mode converters," *Nature Communications*, vol. 5, 2014.

[35] M.-A. Miri, M. Heinrich, R. El-Ganainy, and D. N. Christodoulides, "Supersymmetric optical structures," *Physical Review Letters*, vol. 110, p. 233902, 2013.

[36] Y. D. Chong, L. Ge, and A. D. Stone, "PT-symmetry breaking and laser-absorber modes in optical scattering systems," *Physical Review Letters*, vol. 106, no. 9, p. 93902, 2011.

[37] A. Regensburger, C. Bersch, M.-A. Miri, G. Onishchukov, D. N. Christodoulides, and U. Peschel, "Parity-time synthetic photonic lettices," *Nature*, vol. 488, pp. 167–171, 2012.

[38] L. Feng, Y.-L. Xu, W. S. Fegadolli, M.-H. Lu, J. E. B. Oliveira, V. R. Almeida, Y.-F. Chen, and A. Scherer, "Experimental demonstration of a unidirectional reflectionless parity-time metamaterial at optical frequencies," *Nature Materials*, vol. 12, pp. 108–113, 2013.

[39] S. Rotter and S. Gigan, "Light fields in complex media: mesoscopic scattering meets wave control." under review, 2016.

[40] S. Rotter, J.-Z. Tang, L. Wirtz, J. Trost, and J. Burgdörfer, "Modular recursive Green's function method for ballistis quantum transport," *Physical Review B*, vol. 62, no. 3, pp. 1950–1960, 2000.

[41] F. T. Smith, "Lifetime Matrix in Collision Theory," *Physical Review*, vol. 118, p. 349, 1960.

[42] D. Bohm, *Quantum Theory*. Prentice-Hall, 1951.

[43] E. P. Wigner, "Lower Limit for the Energy Derivative of the Scattering Phase Shift," *Physical Review*, vol. 98, p. 145, 1955.

[44] P. Ambichl, "Delay Times and Beam-Like Scattering States in Coherent Wave Transmission Through Resonators," Master's thesis, TU Wien, 2012.

[45] P. Ambichl, *Delay Times and Beyond In Coherent Wave Transport*. PhD thesis, TU Wien, 2016.

[46] A. A. Juarez, C. A. Bunge, S. Warm, and K. Petermann, "Perspectives of principal mode transmission in mode-division-multiplex operation," *Optics Express*, vol. 20, no. 13, pp. 13810–13824, 2012.

[47] S. Fan and J. M. Kahn, "Principal modes in multimode waveguides," *Optics Letters*, vol. 30, no. 2, pp. 135–137, 2005.

[48] A. Girschik, A. Brandstötter, P. Ambichl, and S. Rotter, "Control of Branched Flow in Optics." in preparation.

[49] I. M. Vellekoop, E. G. van Putten, A. Lagendijk, and A. P. Mosk, "Demixing light paths inside disordered metamaterials," *Optics Express*, vol. 16, no. 1, pp. 67–80, 2008.

[50] J. W. Tay, P. Lai, Y. Suzuki, and L. V. Wang, "Ultrasonically encoded wavefront shaping for focusing into random media," *Scientific Reports*, vol. 4, pp. 3918 EP —-, 2014.

[51] T. Chaigne, J. Gateau, O. Katz, E. Bossy, and S. Gigan, "Light focusing and two-dimensional imaging through scattering media using the photoacoustic transmission matrix with an ultrasound array," *Optics Letters*, vol. 39, 2014.

[52] C. Ma, X. Xu, Y. Liu, and L. V. Wang, "Time-reversed adapted-perturbation (TRAP) optical focusing onto dynamic objects inside scattering media," *Nature Photonics*, vol. 8, no. 12, pp. 931–936, 2014.

[53] H. Cao, "Review on latest developments in random lasers with coherent feedback," *Journal of Physics A: Mathematical and General*, vol. 38, no. 49, p. 10497, 2005.